USGS/NEHRP Award No.: 05HQGR0074

EARTHQUAKE EARLY WARNING FEASIBILITY IN THE BAY AREA

Richard M. Allen

Berkeley Seismological Laboratory, University of California Berkeley,
211 McCone Hall, Berkeley CA 94720.

Tel: (510) 642 1275; Fax: (510) 643 5811; Email: rallen@berkeley.edu

USGS/NEHRP Award No.: 05HQGR0074

Earthquake early warning feasibility in the Bay Area

Richard M. Allen
Berkeley Seismological Laboratory, University of California Berkeley, 211 McCone Hall, Berkeley CA 94720. Tel: (510) 642 1275; Fax: (510) 643 5811; Email: rallen@berkeley.edu

Abstract

Earthquake early warning methodologies can be used to provide a few to tens of seconds warning prior to ground shaking in damaging earthquakes. Warning systems are already in use in Japan, Taiwan, Mexico and Turkey, and in this study we investigate the feasibility of implementing an early warning system in northern California with focus on the San Francisco Bay Area. We consider application of the ElarmS methodology which uses P-wave information to provide an assessment of earthquake hazard as rapidly as possible and then updates the information as time progresses.

Probabilistic warning times are calculated for a series of locations in northern California. The warning time at a set of 26 warning points, such as the San Francisco Civic Center, is estimated for all future likely earthquakes using the ElarmS methodology and the existing seismic networks operated by UC Berkeley and the USGS. For each event, the Working Group on California Earthquake Probabilities (2003) provides an estimate of the probability of occurrence by 2032, and this probability is associated with each warning time. Scenario ShakeMaps for each earthquake also provide an estimate of the likely ground shaking intensity at each warning point for each event. These probabilistic warning time distributions show that warning times range from zero to over a minute. At all locations it is more likely that there will be a warning than not, and most warning times are in the 0-15 sec range although they are typically much larger for the most damaging events.

The ElarmS algorithms are now implemented to run automatically 10 minutes after all M > 3 earthquakes in northern California. This automated processing is the first step to test implementation of the algorithms and is helping us identify necessary improvements in the methodology. Recent earthquakes in the Bay Area provide an important test of how quickly hazard information will be available in case of a large magnitude event in a similar location. The tests show that while warning may not be available to the closest Bay Area city, a warning would be available to the other cities.

We have developed a framework to assess the time dependent errors in predictions of peak ground shaking. The errors for each component of the ElarmS methodology have been determined and can be propagated through the system to estimate the likely error of future prediction. This can be done offline to assess the utility of the warning information for any specific user, and also in realtime during an earthquake to provide information on the likelihood of a false or missed alarm. This framework can also be used to define a critical threshold at which a user should take mitigating action in order to minimize the cost of an earthquake. This threshold is defined in terms of the cost of taking action, the cost of not taking action, the predicted intensity of ground shaking and the uncertainty in the prediction.

Contents

1. Introduction

Earthquake warning systems (EWSs) represent a relatively new approach to seismic risk reduction. They provide a rapid estimate of seismic parameters such as magnitude and location associated with an event. This information can then be used to predict ground motion parameters. EWSs are currently operational in Mexico, Japan, Taiwan and Turkey (Nakamura, 1984; Espinosa Aranda *et al.*, 1995; Wu *et al.*, 1998; Wu and Teng, 2002; Erdik *et al.*, 2003; Odaka *et al.*, 2003; Boese *et al.*, 2004; Kamigaichi, 2004; Nakamura, 2004; Horiuchi *et al.*, 2005). They use a variety of techniques to assess the hazard associated with an earthquake and forward the warning information to users including transportation systems, private industries, public buildings such as schools and government offices, and private residences.

The goal of this project is to assess the feasibility of an EWS in the San Francisco Bay Area. The specific EWS methodology to be assessed is ElarmS. The ElarmS methodology is designed to provide the most rapid assessment of the hazard posed by an earthquake. A first hazard estimate is possible one second after the first P-wave trigger. By using the information contained within the P-wave a warning may be issued before significant ground shaking occurs at the surface, i.e. before the S-wave at the epicenter. The methodology is described by Allen and Kanamori (2003) and Allen (2004), and more information is available on the project website www.ElarmS.org.

The research conducted during the performance period of this NEHRP award falls into four areas which are described in the following sections. First, probabilistic warning times are estimated for future earthquakes in the region. This provides information about the likely warning times available should this system be implemented. Second, the ElarmS methodology has been ported to northern California for the first time. The software can now be run using the data streams available from the Berkeley Digital Seismic Network and the Northern California Network operated by the USGS. Third, we develop a framework for realtime assessment of the errors in a ground shaking prediction. This is achieved by determining the errors associated with each system component as a function of the waveform data available and propagating them through the systm. Finally, we define the threshold at which a specific user should take mitigating action. This is a function of the cost of taking action, the cost of not taking action, the predicted intensity of ground shaking and its uncertainty.

During the performance period of this project, two manuscripts relating to this work were published (Lockman and Allen, 2005; Olson and Allen, 2005), one manuscript is now in press (Allen, in press), and three are in review (Allen, in review; Grasso and Allen, in review; Lockman and Allen, in review). A total of 10 presentations of this work were also made at the International Conference on Urban Disaster Reduction (Allen, 2005), the Chapman Conference on Earthquake Physics (Allen and Olson, 2005), the Earthquake Early Warning Workshop at Caltech (Allen, 2005), AGU (Allen, 2005; Grasso and Allen, 2005; Wurman and Allen, 2005), the Institute of Earth Sciences, Academia Sinica in Taipei, Taiwan, the ANSS Advisory Committee, the Earthquake Hazards Team at the USGS Menlo Park Office and also the Annual Northern California NEHRP meeting.

2. Probabilistic warning times across the Bay Area

Before the utility of an early warning system can be determined, potential users need an assessment of the likely warning times that they can expect to receive in future earthquakes. The warning time in any specific earthquake is dependent on the relative location of the fault rupture and the user, so the range of warning times needs to be assessed. In this study we determine the warning time probability distribution function for locations across California. This is possible using the set of likely earthquakes determined by Working Group on California Earthquake Probabilities (2003). In their study they identified 7 fault systems including 18 rupture segments as shown in Figure 2-1. Different combinations of these segments result in a total of 35 rupture scenarios. The working group estimated the probability of each rupture scenario occurring by 2032. They also calculated scenario ShakeMaps for each event providing an estimate of the expected intensity of ground shaking.

Here we estimate the warning time available for any given location for all earthquake scenarios. The warning time is the difference between the time at which an alert could be available using the ElarmS methodology, and the time at which peak ground shaking occurs at the location of interest. The alert time is defined as the time at which 4 sec of the P-wave have been recorded at the 4 closest seismic stations. Based on previous studies of events in southern California and Japan (Allen and Kanamori, 2003; Lockman and Allen, in review), the average error in the magnitude estimate is less than 0.5 magnitude units when data from 4 stations are available. The stations used are the existing seismic networks run by UC Berkeley and the U.S. Geological Survey. Combined, there are approximately 130 stations with continuous telemetry and either a broadband seismometer or accelerometer as required by the ElarmS methodology (Figure 2-1).

The warning time probability density function (WTPDF) for the city of San Francisco is shown in Figure 2-2. This WTPDF is specifically for the Civic Center; however, it does not vary significantly over the rest of the city. For all the likely damaging earthquakes in the region, San Francisco could receive warnings varying from 77 sec down to -8 sec. Negative warning times mean no warning is possible. The most likely warning times are less than 25 sec; however, the WTPDF has a long tail which is due to the San Andreas Fault. In a repeat of the 1906 earthquake, a 450 km long segment of the fault could rupture. If the event nucleates off the Golden Gate, there would be little or no warning for San Francisco. However, assuming that it is equally likely that rupture nucleates anywhere along the fault, it is more likely that the epicenter is a significant distance from San Francisco and there could be tens of seconds warning for this most damaging earthquake scenario. It should be noted that the 1906 rupture probably did nucleate off the Golden Gate (Bolt, 1968; Boore, 1977; Zoback *et al.*, 1999; Lomax, 2005). Whether this means that a future rupture would nucleate in the same location is unknown.

In addition to the warning times for each earthquake we also estimate the likely intensity of ground shaking at the warning point, i.e. the Civic Center in the case of Figure 2-2. These intensities are derived from ShakeMap scenario calculations (Working

Group on California Earthquake Probabilities, 2003). The grey regions in Figure 2-2 represent earthquakes for which shaking intensity at the Civic Center is less than V on the Modified Mercalli Intensity (MMI) scale (Richter, 1958) and there is unlikely to be damage. Above a MMI V the likely damage increases with the severity of shaking from light (V: unstable objects displaced), to strong (VII: broken furniture and damage to masonry), to violent (IX: masonry seriously damaged or destroyed, frames displaced from foundations). In the case of the WTPDF for San Francisco, Figure 2-2, the long tail of large warning times includes a large portion of the earthquake scenarios which will cause violent (MMI > IX) ground shaking. This is because the intensity of ground shaking in a given earthquake is dependent on the closest distance to the fault rupture, while the warning time is dependent on the distance to the epicenter.

The probability of one or more earthquakes occurring by 2032 for which more or less than a specific warning time could be available is shown in Figure 2-3. The full WTPDF for these locations and other cities and sites of engineering interest are included in the Electronic Supplement. Figure 2-3A shows that there is a 63% probability of one or more earthquakes that will cause some damage (MMI ≥ V) in San Francisco for which a warning would be available, and a 30% chance of a damaging earthquake for which no warning would be available. For the subset of events that cause violent ground shaking (MMI ≥ IX), there is a 3% probability of an earthquake for which > 10 sec of warning could be available, and a 2% chance of < 10 sec warning. It is therefore twice as likely that warning would be available in a damaging earthquake and more likely than not that more than 10 sec warning would be available before violent ground shaking. The WTPDF for the San Francisco International Airport (Figure 2-3B) is similar to that for the city, except that the intensity of ground shaking could be greater given the closer proximity to the San Andreas Fault.

The most severe earthquakes for East Bay cities occur on the Hayward-Rodgers Creek Fault. Its close proximity to cities such as Oakland (Figure 2-1) make for reduced warning times, but also lower intensities due to the shorter length of the fault. It is still more likely than not that a warning will be available for a damaging earthquake, Figure 2-3D. Most of the hazard for San Jose comes from the San Andreas Fault. As with San Francisco, this means there is a high probability of large warning times for the most damaging earthquakes. There is a 3% probability of an event causing MMI VIII in San Jose for which > 20 sec warning could be available, more than the 2% chance of < 20 sec warning (Figure 2-3E). In the October 17, 1989, Loma Prieta (M_w 6.9) earthquake Santa Cruz experienced MMI VIII. There is a 7% probability of a similar intensity of ground shaking by 2032 in Santa Cruz, and a 3% chance of similar ground shaking for which > 30 sec warning could be available (Figure 2-3C). Finally, the rapidly growing urban areas east of the Berkeley Hills, such as Walnut Creek, are as likely to experience damaging ground shaking as San Francisco, although the most severe events have a lower intensity (Figure 2-3F). As is the case for all locations in the SFBA, Walnut Creek could receive a warning before ground shaking starts for the majority of damaging earthquakes.

This study shows that for a specific city, such as San Francisco, the warning time could be tens of seconds for some earthquakes while being zero seconds for others. However,

in situations when San Francisco gets zero seconds warning, Oakland would likely get a few seconds and San Jose would get ~15 sec warning. Thus, for any earthquake scenario in a densely populated region, such as the San Francisco Bay Area (SFBA), an EWS could provide warning to at least some of the affected population in a damaging earthquake. The probability functions also provide the necessary information for potential users to determine the effectiveness of implementing mitigation strategies that use early warning information.

This work is now in press for Seismological Research Letters (Allen, in press). A preprint of the full manuscript in included in Appendix A. The warning time probability density functions for many other cities, airports and other sites of engineering interest are available online at http://seismo.berkeley.edu/~rallen/pub/2005wtpdfsf/esup/

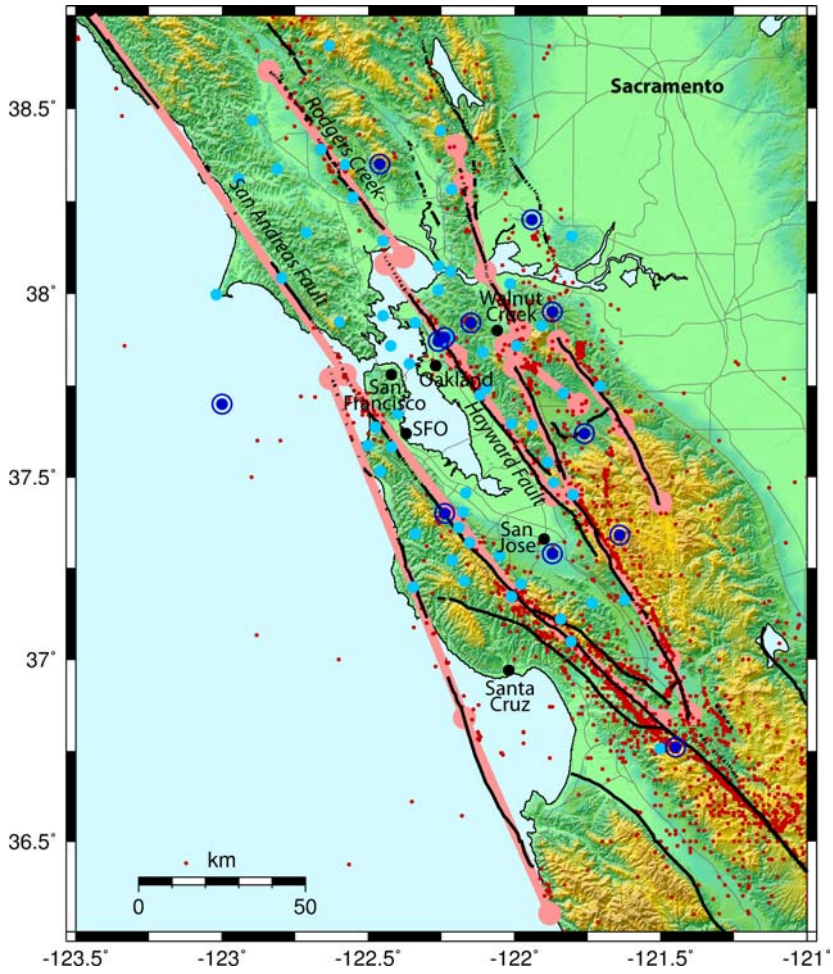

Figure 2-1. Map of the study region showing mapped faults (bold black lines) and the location of earthquakes with magnitude greater than 3 since recording began (red dots). Existing continuous broadband stations operated by UC Berkeley (dark blue) and the U.S. Geologic Survey (light blue) are shown with circles for broadband velocity seismometers and dots for accelerometers. The fault segments identified by the Working Group on California Earthquake Probabilities (2003) are shown with pink dots at the ends of segments joined by broad pink lines. The six "warning points" included in Figures 2-2 and 2-3 are shown as black dots.

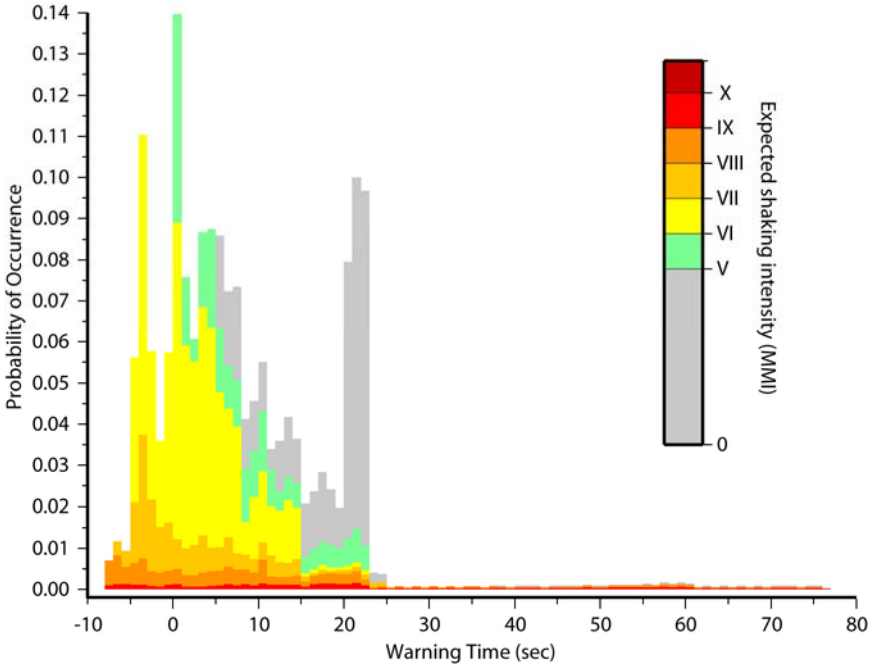

Figure 2-2. Warning time probability density function (WTPDF) for the Civic Center of San Francisco (37.78°N, 122.42°W). The warning times for all likely earthquakes range from -8 sec to 77 sec, where negative warning times mean no warning is possible. Earthquakes are in 1 sec bins and the vertical axis shows the total probability of one or more earthquakes occurring before 2032 with a given warning time. The color represents the estimated intensity of ground shaking for each event. Damage is unlikely for MMI < V (grey); MMI > IX means violent shaking likely to cause serious damage to buildings (red).

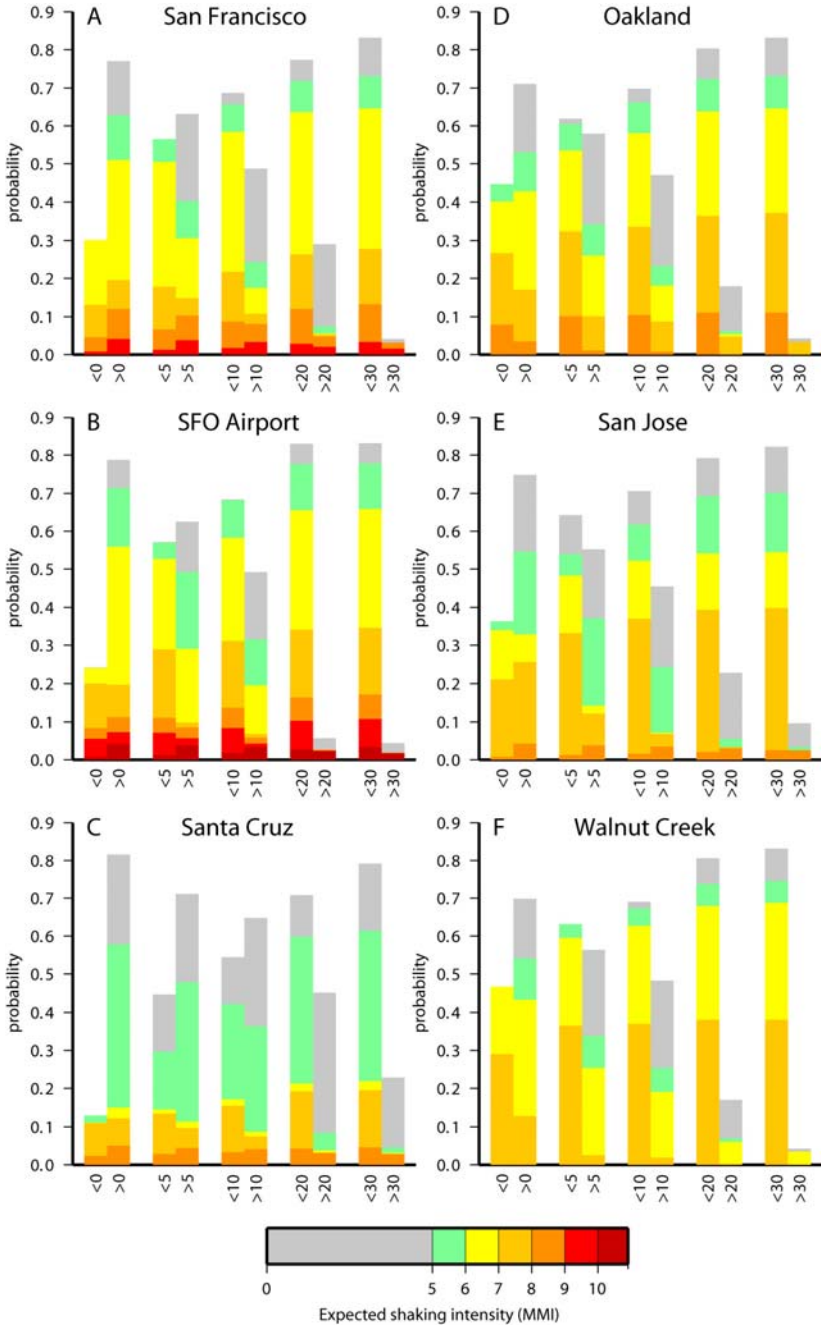

Figure 2-3. Probability that one or more earthquakes will occur by 2032 for which more or less than 0, 5, 10, 20 and 30 sec warning time could be available. The probabilities for six locations around the SFBA are shown for comparison. The color indicates the intensity of ground shaking expected. The six locations are shown on Figure 2-1. A) The city of San Francisco (37.78°N, 122.42°W), B) San Francisco International Airport, SFO (37.62°N, 122.37°W), C) The city of Santa Cruz (36.97°N, 122.03°W), D) The city of Oakland (37.805°N, 122.270°W), E) The city of San Jose (37.33°N, 121.90°W), F) The city of Walnut Creek (37.90°N, 122.06°W).

3. Application for ElarmS across the Bay Area

Over the past year the ElarmS algorithms have been adapted and ported to the seismic systems in northern California. In January 2006 ElarmS began operating in a fully automatic fashion at the Berkeley Seismological Laboratory. The automatic processing is initiated by a notification e-mail sent by the Rapid Earthquake Data Integration (REDI) system following an event detection. There is a built-in delay of 10 minutes following receipt of the e-mail to allow for the requisite data to arrive at the network data center. After this delay, the data is retrieved from the data center and processed using the ElarmS algorithms with no human interaction. When this processing is complete, the system notifies an operator by email and the event may be subsequently reviewed by a human. However, no human input is used to detect, locate or estimate the size of any event.

Since January 2006, the ElarmS automatic code has processed 19 events in Northern California, ranging in magnitude from 2.9 to 4.6. Three of these events have been local to the SFBA (see Figure 3-1), and have served as test cases for rapid warning for Bay Area events. A summary of ElarmS' performance is presented in Table 3-1, with the Bay Area events in italics. In our initial testing we only trigger an "alarm" when 4 sec of data are available at 4 stations (the same alarm criteria as used in section 2). Information about an event is available before this time, although with greater uncertainty. Of the 19 events that occurred since January 2006, 9 successfully triggered an alarm. There are two reasons for having over 50% missed alarm rate for these events. The principal cause of this is a lack of instrumental coverage. Due to poor signal-to-noise ratio for small events (M<5), strong motion stations are unusable for magnitude determination of small events. Thus, most of the NCSN strong motion sites in the Bay Area are removed from the process and cannot contribute to early warning for these events.

A second reason is the poor triggering performance realized by the simple STA-LTA algorithm currently in use by ElarmS. We are currently working toward a real-time implementation of an autoregressive triggering algorithm (Sleeman and van Eck, 1999) to improve our trigger performance. This should markedly improve the performance of the system for small events. Additionally, a large source of error when calculating magnitude from strong motion data is late triggering caused by low signal-to-noise ratio, and the improved triggering algorithm may improve performance enough to bring some strong motion data back into the calculations for moderate-size events.

Another observation is that ElarmS characteristically underpredicts the magnitude of these small events. This is due again to lower signal-to-noise ratio at magnitudes less than 5, the effects of which are apparent even in the high-gain broadband data. We are currently investigating several different algorithms for calculating the predominant period of the P-wave arrival, which may help to reduce this measurement's susceptibility to noise or pollution of the signal by other seismic phases or sources.

An example event in the Bay Area

Three events in Table 3-1 merit particular attention, as they occurred within the Bay Area. The performance of ElarmS in these cases represents likely future performance in

the case of a large event with a similar epicenter. We will examine one of these, a M_W 3.7 event, which occurred near Moraga, CA on 21 March 2006. Figure 3-2 shows four time slices between the initial detection of the event and the triggering of an alarm.

In the first time slice, four seconds after the event origin, the first P-wave has been detected at station BRIB. For the time being, ElarmS locates the event directly under the station. There is no estimate of the magnitude yet, because this requires at least one second of P-wave data at station BRIB, which is not available yet. The numbered rings around the epicenter represent the time in seconds until the onset of peak ground motions at all locations around the event.

In the second slice, five seconds after the event origin, the first magnitude estimate becomes available from the first second of P-wave data at station BRIB. The initial estimate is magnitude 1.1, but this will change as more data becomes available. The colors around the epicenter represent predicted peak ground velocity based on an empirical radial attenuation relationship. Note also that the location of the event has shifted significantly, because two more stations have reported triggers in the last second; stations BKS and BRK. When two stations have reported triggers, ElarmS provisionally locates the event between the two stations based on the relative trigger times. When three or more stations report triggers, ElarmS performs a grid search to find the best location for the event.

In the third slice, six seconds after the event origin, a fourth station, BDM, has reported a trigger. After four more seconds, when four seconds of P-wave data are available at BDM, an alarm would be issued based on the information available at that time. Note that the location of the event has moved back toward the actual epicenter as a result of incorporating the fourth station's trigger time in the grid search. Note also that the magnitude estimate has increased to 1.5 as a result of an additional second's data at BRIB and the first second of data from BKS and BRK becoming available. Finally, note that station BRIB has turned black, indicating that it has entered the peak ground motion window. When this has passed, BRIB will report an observed peak ground acceleration, which will be used to scale the predicted ground motions up or down for all other locations. Over the next three seconds, data from these four stations as well as from station WENL will increase the magnitude estimate and refine the location of this event.

In the final time slice, 10 seconds after the event origin, 4 sec of P-wave data are available at 4 stations and an alarm would be issued. Note that station BRIB is light blue, corresponding to a reported peak ground acceleration of around 5 cm/s^2. BKS and BRIB report around 1 cm/s^2 and appear white. Station BDM is experiencing peak ground motion at this time, and stations WENL to the southeast and JRSC to the southwest have triggered (station JRSC only triggered this second, and does not contribute to the magnitude estimate). The current magnitude estimate is 3.5, within 0.2 magnitude units of the moment magnitude determined later. The numbered rings indicate that San Francisco is just beginning to experience peak ground shaking, and San Jose has between 5 and 10 seconds of warning from this moment. It is important to note, however, that these figures do not take into account any telemetry delays associated

with transmitting data from the seismic stations to the network data center, or those associated with disseminating an alarm to the public.

Although there are a number of issues yet to be resolved before ElarmS can be used in a real-time setting, the system performs reasonably well and can potentially provide 5 to 10 seconds of warning time to most of the Bay Area in the event of a local earthquake. Low signal-to-noise ratio at small magnitudes is a problem in that a small event may be miscalculated to be a hazardous larger event due to noise, increasing the probability of false alarms. By working to reduce the sensitivity of ElarmS to noise and polluted signals, this effect should be minimized, and with the addition of strong-motion stations to the detection system, warning times will be further increased.

Date Alarm Delay (s)	Origin Time Time Error (s)	N Latitude E Longitude Position Error (km)	Network Mag ElarmS Mag Magnitude Error
2006/02/04 *15*	*18:05:02.26* *0.97*	*37.4672* *-121.815* *4.03*	*3.14* *2.50* *-0.64*
2006/02/04 *	18:47:26.20 *	40.3727 -124.544 *	2.89 * *
2006/02/06 *	04:55:39.29 *	35.8192 -119.913 *	3.21 * *
2006/02/16 *	17:47:59.65 *	37.9848 -118.773 *	4.25 * *
2006/02/18 10	12:38:16.01 1.05	37.8135 -122.072 1.94	3.24 2.59 -0.65
2006/02/23 *	15:10:38.93 *	38.8267 -122.804 *	3.22 * *
2006/02/24 *	23:54:47.45 *	40.2297 -121.167 *	3.17 * *
2006/02/25 *	12:15:50.60 *	38.3543 -119.42 *	3.00 * *
2006/03/01 *14*	*19:34:52.09* *0.76*	*37.8577* *-122.21* *2.76*	*3.36* *2.97* *-0.39*
2006/03/02 20	00:11:55.15 0.67	36.5562 -121.148 10.85	3.17 2.35 -0.82
2006/03/02 *	04:53:31.31 *	40.4337 -125.457 *	2.86 * *
2006/03/03 *	12:49:50.95 *	39.0315 -123.114 *	3.69 * *
2006/03/05 20	05:32:24.18 1.05	36.6005 -121.054 2.34	2.94 2.67 -0.27
2006/03/08 *	02:11:00.87 *	36.5612 -121.146 *	3.03 * *
2006/03/21 *10*	*21:41:42.24* *1.19*	*37.8088* *-122.073* *2.27*	*3.70* *3.54* *-0.16*
2006/03/23 *	10:17:23.44 *	38.7693 -122.733 *	2.98 * *
2006/03/23 19	12:55:28.74 1.19	35.7003 -121.022 4.19	2.97 2.34 -0.63
2006/03/25 19	04:21:10.12 1.18	35.6545 -121.082 4.37	3.19 1.94 -1.25
2006/03/26 15	01:56:38.20 3.57	40.2732 -124.386 26.53	4.60 3.20 -1.40

Table 3-1: Performance summary of automated ElarmS in Northern California. Alarm delay is the number of seconds after the actual origin time that an alarm would trigger. An alarm triggers when 4 seconds of P-wave data are available at 4 stations. Time error is the difference between actual origin time and that determined using trigger data. Position error is the distance between the actual epicenter and that determined using trigger data. All errors are determined at the time that the alarm triggers. Network magnitude may be either duration, local, or moment magnitude. Asterisks (*) indicate that no alarm triggered for this event. Events in the Bay Area are in italics.

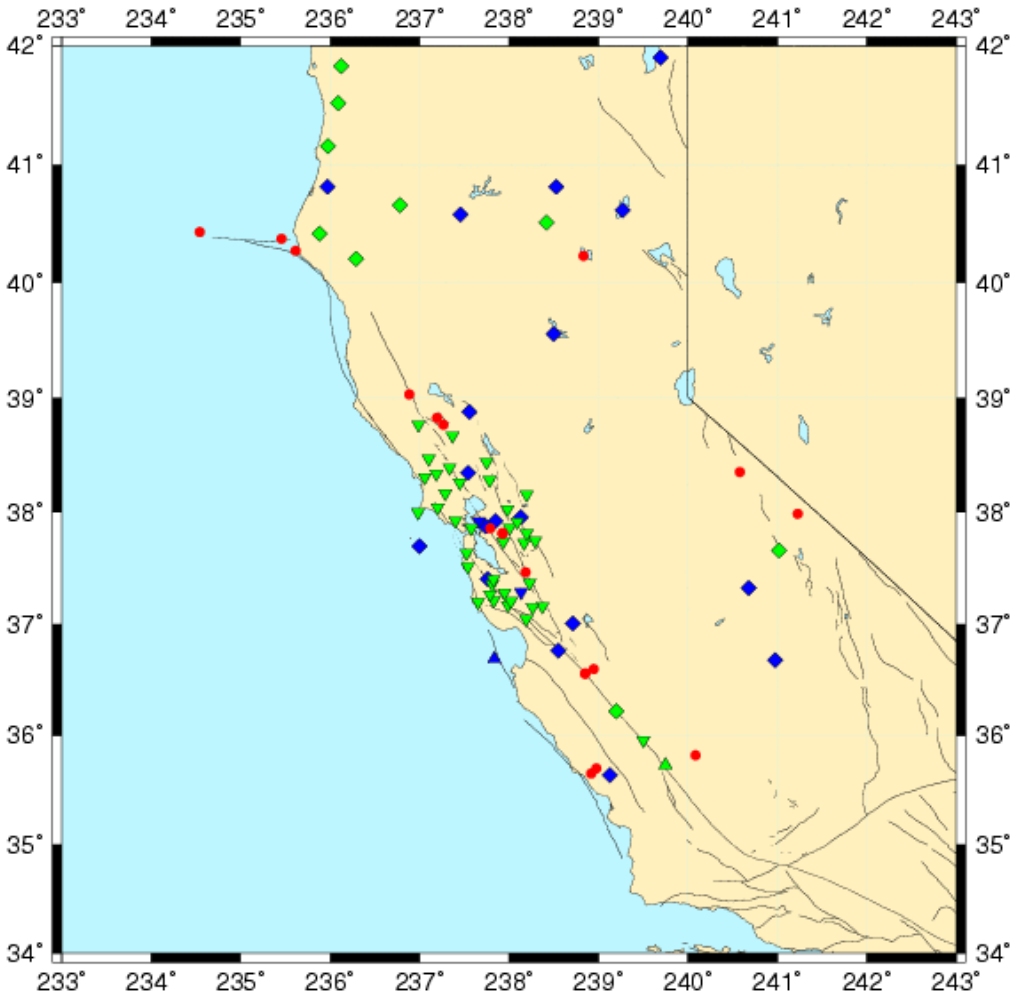

Figure 3-1. A map of station distribution in Northern California, with events since January 2006 in red. Green and blue symbols represent NCSN and BDSN stations, respectively, and the shape of the symbol represents the type of instrument; triangles represent broadband velocity instruments, inverted triangles represent strong motion accelerometers, and diamonds represent a collocation of both instruments.

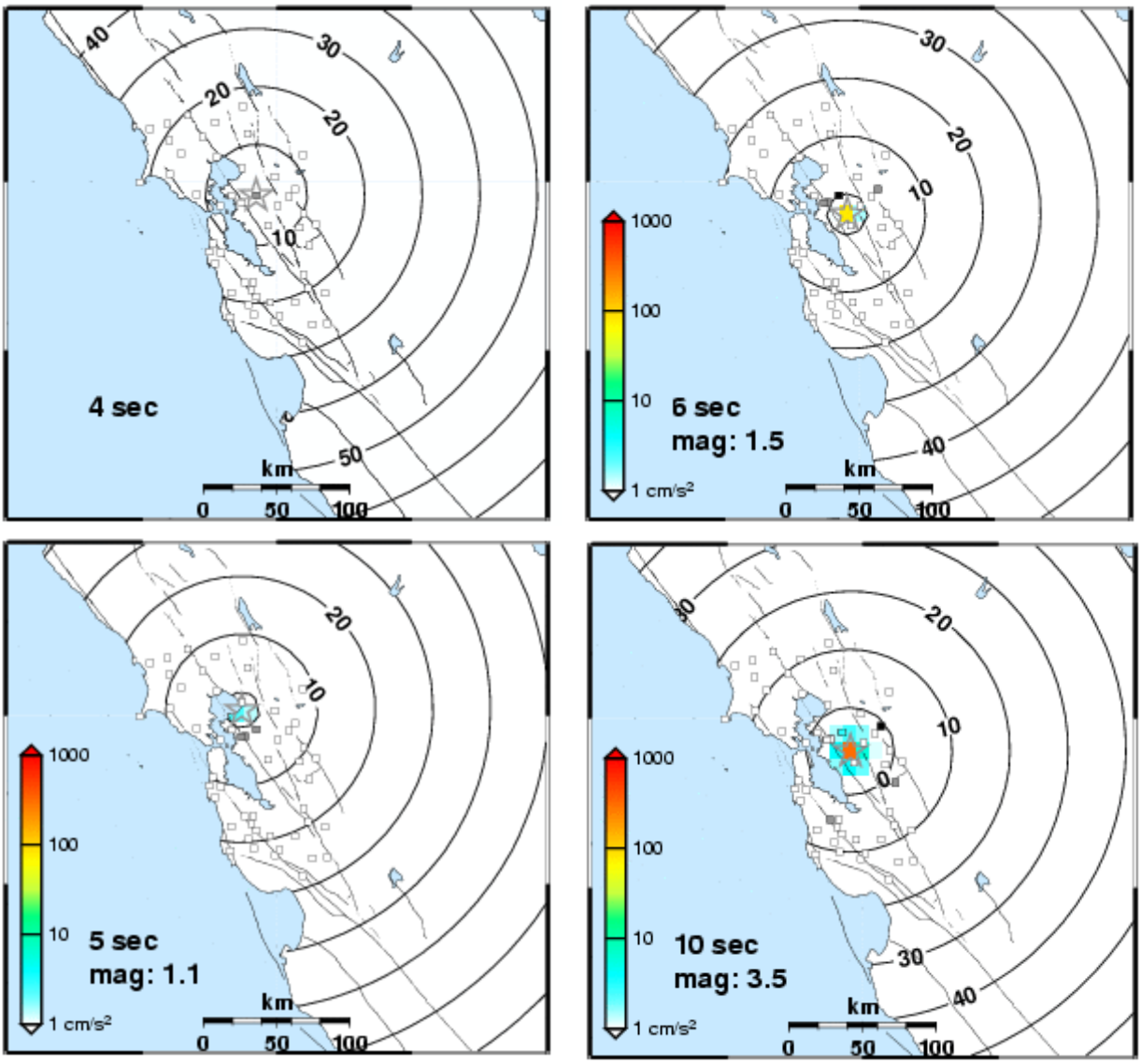

Figure 3-2: Four time slices of a M_W 3.7 event near Moraga, CA, as it was processed automatically by ElarmS. Grey stations are those reporting triggers, black stations are experiencing peak ground motions, and colored stations report ground motion according to the scale on the left side. The numbered rings represent the time in seconds until the onset of peak ground shaking at all locations on the map, while colors on the background map represent predicted ground motions based either on the estimated magnitude or on the observed ground motions at seismic stations.

4. Uncertainty in real-time predictions

The ElarmS methodology can be represented as a multi-component model consisting of earthquake location, magnitude estimation and ground shaking prediction. The total uncertainty in a ground motion prediction can be derived from the individual errors in location, magnitude estimates using the predominant period, and the attenuation relations.

To assess these errors we use a dataset of 32 earthquakes from southern California. The event dataset consists of earthquakes recorded by the current dense seismic network close to the metropolitan areas and have a local magnitude ranging from 3.0 to 5.4. The dataset does not include larger magnitude earthquakes as none have occurred beneath a dense seismic network as exists today. The waveforms were recorded by the California Integrated Seismic Network (http://www.cisn.org) and were obtained from the Southern California Earthquake Data Center (http://www.data.scec.org).

Magnitude uncertainty

We determine the error in the ElarmS magnitude estimate as a function of time for the 32 events. The error is defined as the difference between the magnitude estimate provided by ElarmS and the true magnitude determined by the network. The time of the first trigger for each event is set to the zero time. In making this choice we assume that the amount of information about an earthquake, i.e. the number of stations recording P-wave information, increases in a similar fashion with time for all earthquakes. This assumption is reasonable for events occurring beneath the dense portion of the seismic network where the station spacing is approximately constant.

We find that the magnitude error follows a Gaussian distribution. For each 1 sec increment an error model is determined by fitting a Gaussian distribution to the errors to determine the mean and standard deviation. Figure 4-1 shows that the error decreases as a function of time. Initially the magnitude estimate is low and the error large with a mean and standard deviation of -0.45 and 0.61 respectively. Hereafter, we refer to mean and standard deviations as -0.45 ± 0.61. The values decrease to -0.25 ± 0.41 after 5 sec, -0.14 ± 0.34 after 10 sec, and stabilize at -0.05 ± 0.26 at 15 sec (Figure 4-1). Clearly the greatest improvements in the magnitude estimate occur within the first few seconds as the number of triggered stations increases from 1 due to improved accuracy with increasing stations. The magnitude estimation methodology will also inherently give a low magnitude estimate initially as the maximum predominant periods characteristic of large events are observed at greater times after the P-wave trigger than those for small events (Olson and Allen, 2005). An event will therefore appear to be small initially and the magnitude estimate will increase with time (Allen and Kanamori, 2003).

Location uncertainty

The location error is defined as the scalar distance between the estimated epicenter and the true network epicentral location. We calculate the location errors for the 32 earthquakes at 1 second increments and determine the best fit lognormal distributions. These distributions are shown in Figure 4-2. We find that the location error is reduced

to within 1 km within a few seconds. Given 1 trigger an event is located at the station to trigger which would mean that a typical location error would be ~7 km (given the typical station spacing of 20 km). At 1 sec, however, the error is 1.41 ± 1.02 km which is significantly lower. This is because information is assimilated in 1 second increments and the station density results in typically two or three triggers to occur within the first second making for accurate location estimates very quickly.

Attenuation model uncertainty

The attenuation model error is the difference between the predicted peak ground acceleration (*PGA*), and the observed *PGA* recorded during the course of the earthquake. The error in the attenuation relationship represents the error in the *PGA* prediction given the correct magnitude and distance. We find that the attenuation relationship error can be approximated by a Gaussian distribution and the best fit Gaussian to the errors for all 32 earthquakes are shown in Figure 4-3. The error distributions are similar for all the events, with means around zero. The errors for all events are combined to determine a single Gaussian error distribution for the attenuation relations. It has a mean of 0.26 and standard deviation equal to 0.9 (Figure 4-3).

Error analysis

To simulate the errors in ground shaking predictions generated by ElarmS we propagate the errors through the system. The estimated value of peak ground acceleration, $\hat{PGA}$, is a function of the estimated magnitude, $\hat{M}$, and the estimated epicentral distance, $\hat{R}$:

$$\hat{PGA} = f(\hat{M}, \hat{R}) \tag{4-1}$$

where *f* represents the attenuation relationship. $\hat{M}$ and $\hat{R}$ are estimated from the true magnitude *M*, the true epicentral distance *R*, using their time dependent errors ε_M, ε_R (Figures 4-1 and 4-2) respectively:

$$\begin{aligned} \hat{M} &= M + \varepsilon_M \\ \hat{R} &= R + \varepsilon_R \end{aligned} \tag{4-2}$$

thus

$$\hat{PGA} = f(M + \varepsilon_M, R + \varepsilon_R) \tag{4-3}$$

The error in the *PGA* prediction, ε_{PGA}, is determined by differencing the logarithm of the observed and the predicted *PGA*:

$$\varepsilon_{PGA} = \log\left(\hat{PGA}\right) - \log(PGA) = \log\left(f(M + \varepsilon_M, R + \varepsilon_R)\right) - \log(PGA) \tag{4-4}$$

We use the difference in the logarithm of the *PGA* observation to account for the wide range of *PGA* values given the range of magnitudes for the dataset. This is typical in studies of ground shaking attenuation.

A Monte Carlo simulation is used to estimate the total uncertainty in ε_{PGA}. The 32 earthquake dataset consists of a total of 2961 observations of *PGA* for which *M* and *R* are known. For each of these data we run 1000 simulations from 1 to 25 seconds. For each time increment $\hat{M}$ and $\hat{R}$ are estimated using equation (4-2) and randomly choosing errors from their time-dependent distributions to generate $\hat{PGA}$. ε_{PGA} is then calculated using the predicted and observed *PGA*.

The uncertainty associated with the ground motion parameter prediction follows a Gaussian distribution with mean and standard deviation that vary with time as shown in Figure 4-4. The mean is low initially due to the conservative estimate of magnitude as described above, but rapidly increases from -0.61 at 1 sec to -0.17 at 5 sec. The standard deviation decreases a little with time from 1.33 at 1 sec to 0.95 at 20 sec.

Sensitivity analysis
To determine the largest source of error in the PGA predictions we conduct a simple sensitivity analysis. The total error in the PGA prediction can be espressed as

$$\varepsilon'_{PGA} = \log\big(f(M+\varepsilon_M, R+\varepsilon_R)\big) + \varepsilon_{Att} - \log\big(f(M,R)\big) \qquad (4\text{-}5)$$

where ε'_{PGA} is the error in the PGA estimate calculated using the error models rather than the observed PGA (which was the case in equation 4-4), and ε_{Att} is the error in the attenuation relations which is Gaussian with mean 0.26 and standard deviation equal to 0.9 as described above.

We consider four cases. In case 1 we include all three sources of error in equation 4-5. The characteristics of ε'_{PGA} are shown in Figure 4-5. In case 2 we set the error in the magnitude estimate, ε_M, to zero thereby assuming an exact magnitude is available for an event and ε_R and ε_{Att} are the only sources of error in ε'_{PGA}. Figure 4-5 shows ε'_{PGA} as a function of time. Comparing case 2 to case 1 (Figure 4-5) the most important difference is that the mean in case 2 is no longer initially low. The low initial estimate in ground shaking is a product of the low initial magnitude estimate which is a design element of ElarmS. The standard deviation in case 2 is 0.9 at all times. This is a marginal improvement on the standard deviation for case 1 at ≤ 10 sec and similar at later times. It is also equal to the standard deviation for the attenuation models.

In case 3 the epicentral distance estimate is assumed to be accurate while ε_M and ε_{Att} are sources of error. Figure 4-5 shows that the errors for case 3 are very similar to case 1 indicating that errors in epicentral distance are not a significant contribution to the overall error. Finally, in case 4 ε_{Att} is set to zero and we consider errors in ε_M and ε_R

only. In this case (Figure 4-5) the mean error parallels the error for case 1 but is always lower starting at -0.91 at 1 sec and increasing to -0.14 at 20 sec. The standard deviation is significantly lower than case 1 except for the first few seconds. This shows that ε_{Att} dominates ε'_{PGA} after 5-10 sec.

In summary, ε_R has a negligible contribution to uncertainty in PGA predictions, ε_M contributes initially (the first 5-10 sec), and ε_{Att} is the most significant source of error, particularly at later times after several stations have recoded P-wave arrivals and contribute to the magnitude estimate. An important conclusion of this study is that the attenuation relations are currently the largest source of error in the PGA predictions, not the rapid magnitude determination. Further development of the system should therefore focus on improved attenuation relations. It should be noted that the current attenuation relations are very simple.

Additional information about this study is available in Appendix B which contains a manuscript currently in review (Grasso and Allen, in review).

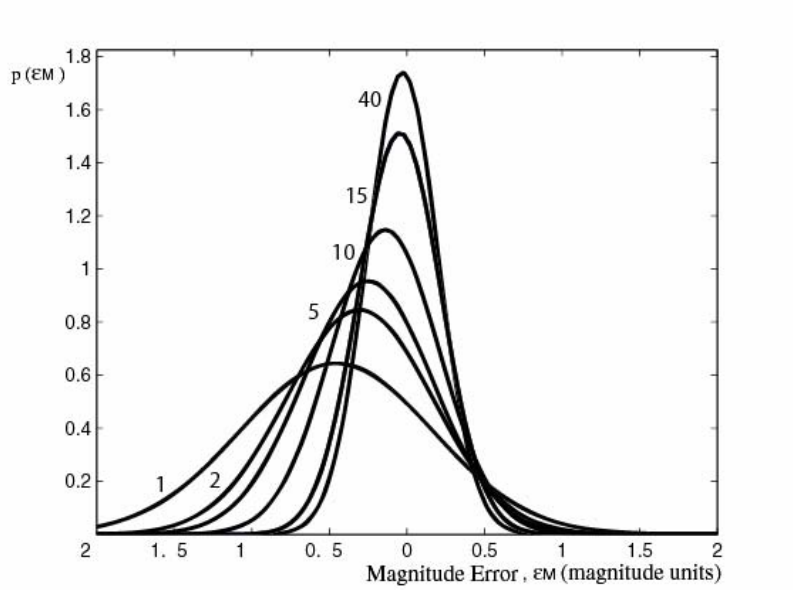

Figure 4-1. Magnitude error distributions as a function of time. The labels show the time in seconds with respect to the time of the first station to trigger. The mean and standard deviations for each Gaussian distribution are shown in Table 4-1.

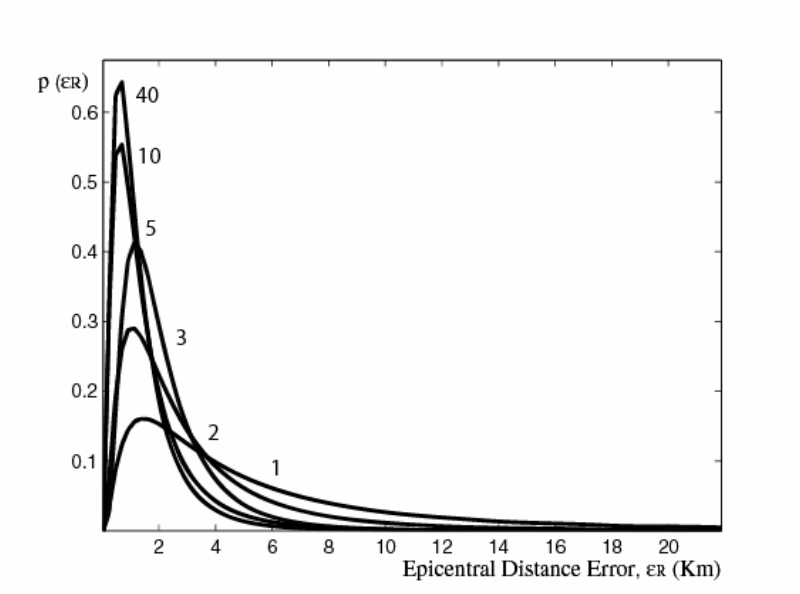

Figure 4-2. Location error distributions as a function of time. The labels show the time in seconds with respect to the time of the first station to trigger. The mean and standard deviations for each lognormal distribution are shown in Table 3.

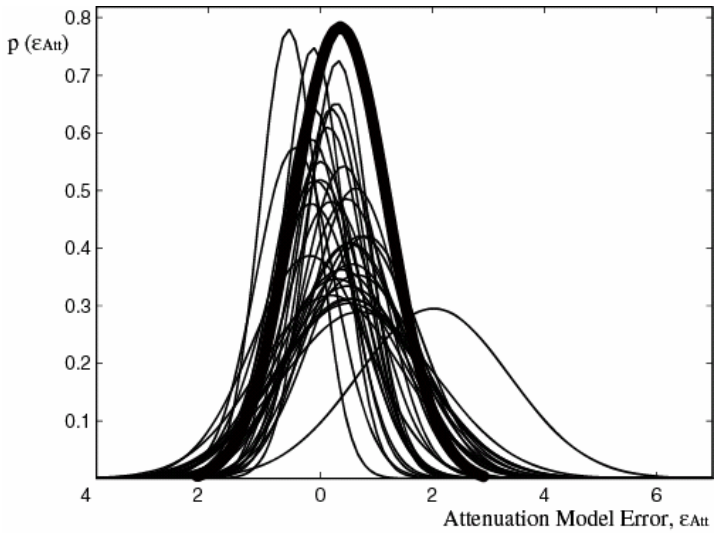

Figure 4-3. Attenuation model uncertainty. The distributions for each of the 32 earthquakes are shown as thin lines. The distribution for all data is shown as the bold line. See text for definition of attenuation model error.

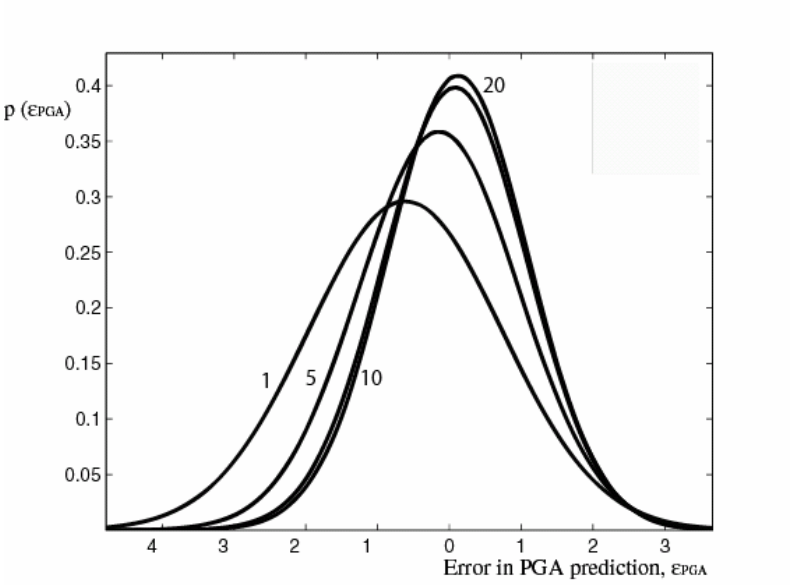

Figure 4-4. Total error in PGA predictions as a function of time. The labels show the time in seconds with respect to the time of the first station to trigger.

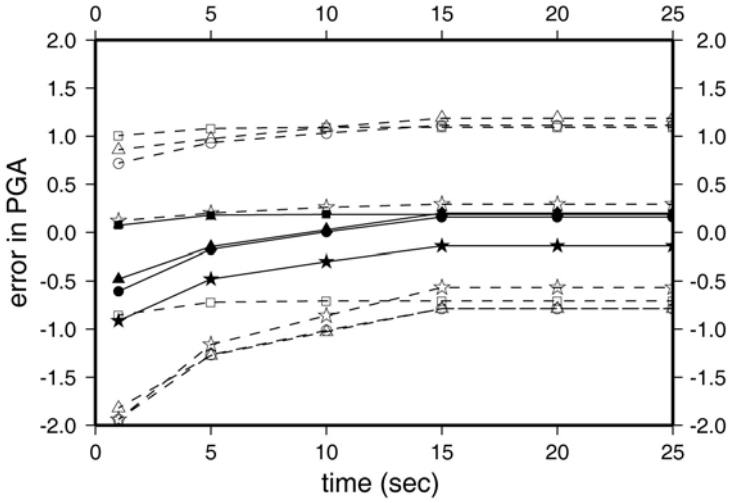

Figure 4-5. Error in PGA as a function of time for the four cases. The mean is shown as a solid symbol joined by a solid line, plus and minus one standard deviation are shown with open symbols joined by a dashed line. Case 1 (circles) includes all sources of error. Case 2 (squares) neglects error in the magnitude estimate, ε_M, but includes epicentral distance error, ε_R, and the attenuation relation error, ε_{Att}. Case 3 (triangles) neglects ε_R but includes ε_M and ε_{Att}. Case 4 (stars) neglects ε_{Att} but includes ε_M and ε_R.

5. Application of warning information

A user of early warning information needs a framework within which to decide at what point during an earthquake mitigating action should be taken. This critical threshold is dependent on the cost of taking action, the cost of not taking action, the predicted ground shaking intensity and the certainty of the prediction. A cost-benefit analysis can be used to determine this threshold and here we outline how this can be done.

As a consequence of the uncertainty associated with the prediction, we may commit errors of two kinds: false and missed alarms. A missed alarm occurs if we do not activate the alarm when we should have activated it. A false alarm occurs when we activate the alarm when we should not have. The critical threshold, *a*, for a facility is the intensity of ground shaking at which unacceptable damage or injury will occur. The warning threshold at which mitigating actions should be taken is defined as *ca,* where *c* is a coefficient. If false alarms are not a serious concern and the consequences of *PGA* exceeding *a* are, then *c* will be a small number less that one. If the reverse is true and false alarms are highly costly, then *c* should be larger than one. Figure 5-1 schematically shows the inherent trade-off between false and missed alarms. The total uncertainty, ε'_{PGA}, in the prediction is represented by the width of the data points in Figure 5-1. *a* and *ca* are indicated on the PGA and $P\hat{G}A$ axes respectively. If the value of *c* is increased then the number of false alarms is reduced but at the cost of increased missed alarms.

At any time during an earthquake the probability of a false alarm, P_{fa}, or missed alarm, P_{ma}, can be calculated given the error distribution of $P\hat{G}A$:

$$\begin{aligned} P_{fa}(t) &= P\left[PGA < a \mid P\hat{G}A(t)\right] \\ P_{ma}(t) &= P\left[PGA \geq a \mid P\hat{G}A(t)\right] \end{aligned} \tag{5-1}$$

where the probability distribution function $P(PGA \mid P\hat{G}A)$ is a Gaussian distribution with mean $P\hat{G}A + \mu_{\varepsilon'_{PGA}}$ and standard deviation $\sigma_{\varepsilon'_{PGA}}$ given by the above error analysis. The threshold in terms of tolerable probability of false alarm at which action should be taken can be defined in terms of the ratio of costs of false alarm, C_{fa}, to the savings made by activating the alarm when the ground shaking then exceeds the critical threshold, C_s. We define the threshold, β, in terms of this cost ratio:

$$\beta = \frac{C_s}{C_{fa} + C_s} \tag{5-2}$$

A facility can minimize the costs associated with earthquakes by activating the alarm and mitigation steps when $P_{fa} < \beta$. The same cost-benefit analysis can be used to define

c, in which case activating the alarm when $P\hat{G}A > ca$ is equivalent to activating it when $P_{fa} < \beta$.

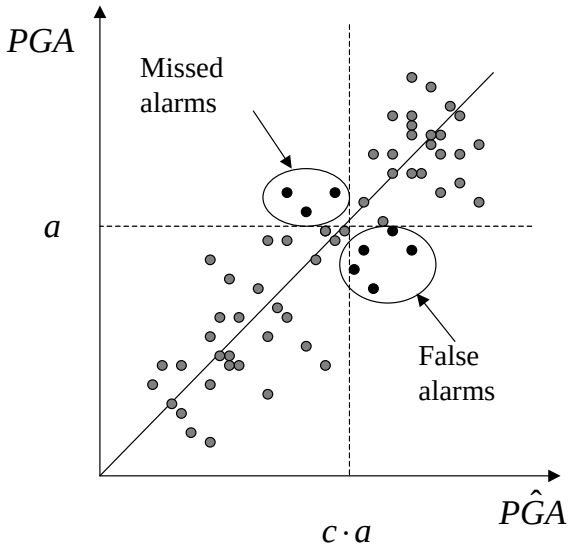

Figure 5-1. Schematic showing the distribution of errors in *PGA* predictions with respect to the observed *PGA*. The critical threshold, *a*, is shown along with a warning threshold, *ca*. The false and missed alarms are indicated. The number of false alarms can be reduced by increasing the value of *c*. However, the number of missed alarms will also increase.

6. Summary

Active earthquake warning systems are now operational in Mexico, Japan, Taiwan and Turkey (Nakamura, 1984; Espinosa Aranda *et al.*, 1995; Wu *et al.*, 1998; Wu and Teng, 2002; Erdik *et al.*, 2003; Odaka *et al.*, 2003; Boese *et al.*, 2004; Kamigaichi, 2004; Nakamura, 2004; Horiuchi *et al.*, 2005). Their warning messages are currently used by transportation systems such as rail and metro systems, as well as private industries, including construction, manufacturing and chemical plants. They are also used by utility companies to shut down generation plants and dams, and emergency response personnel to initiate action before ground shaking. In addition, schools receive the warnings allowing children to take cover beneath desks, housing units automatically switch off gas and open doors and windows, and entire complexes evacuate.

The various studies described in this final report have taken the next step toward providing short-term earthquake mitigation in California as has already been done in other earthquake prone regions. The probabilistic warning times show that the range of warning times is zero to over a minute and that warning would be available to many people in most earthquakes. The ElarmS methodology has now been implemented in northern California and runs automatically after an earthquake. Continuing assessment of its performance after each earthquake allows further development of improvements in the methodology. The error framework now developed is also providing information on which components of the warning system should be the focus of further development. The framework will also be made available to potential users of the warning information as they assess how they could use this information.

7. Cited References

Allen, R. M. (2004). Rapid magnitude determination for earthquake early warning, in *The many facets of seismic risk* eds M. Pecce, G. Manfredi and A. Zollo, Universita degli Studi di Napoli "Federico II", Napoli, 15-24.

Allen, R. M. (2005). Application of elarms across california, *Earthquake early warning workshop*, Caltech, California,

Allen, R. M. (2005). Earthquake early warning in northern california, *EERI/ISSS First International Conference on Urban Disaster Reduction*, Kobe, Japan,

Allen, R. M. (2005). The relation between rupture initiation and earthquake magnitude, *AGU Fall Meeting*, San Francisco, California,

Allen, R. M. (in press). Probabilistic warning times for earthquake ground shaking in the san francisco bay area, *Seis. Res. Lett.*

Allen, R. M. (in review). The elarms earthquake warning methodology and application across california, in *Seismic early warning* eds P. Gasparini and J. Zschau, Springer,

Allen, R. M. and H. Kanamori (2003). The potential for earthquake early warning in southern california, *Science* **300,** 786-789.

Allen, R. M. and E. L. Olson (2005). The deterministic nature of earthquake rupture? *Chapman Conference: Radiated Energy and the Physics of Earthquake*, Portland, Maine,

Boese, M., M. Erdik and F. Wenzel (2004). Real-time prediction of ground motion from p-wave records, *Eos Trans. AGU Fall Meet. Suppl.* **85,** Abstract S21A.0251.

Bolt, B. A. (1968). The focus of the 1906 california earthquake, *Bull. Seismol. Soc. Am.* **50,** 457-471.

Boore, D. M. (1977). Strong-motion recordings of california earthquake of april 18, 1906, *Bull. Seismol. Soc. Am.* **67,** 561-577.

Erdik, M. O., Y. Fahjan, O. Ozel, H. Alcik, M. Aydin and M. Gul (2003). Istanbul earthquake early warning and rapid response system, *Eos Trans. AGU Fall Meet. Suppl.* **84,** Abstract S42B.0153.

Espinosa Aranda, J. M., A. Jimenez, G. Ibarrola, F. Alcantar, A. Aguilar, M. Inostroza and S. Maldonado (1995). Mexico city seismic alert system, *Seismo. Res. Lett.* **66,** 42-52.

Grasso, V. F. and R. M. Allen (2005). Earthquake warning systems: Characterizing prediction uncertainty, *AGU Fall Meeting*, San Francisco, California,

Grasso, V. F. and R. M. Allen (in review). Uncertainty in real-time earthquake hazard predictions,

Horiuchi, S., H. Negishi, K. Abe, A. Kamimura and Y. Fujinawa (2005). An automatic processing system for broadcasting earthquake alarms, *Bull. Seismol. Soc. Am.* **95,** 708-718.

Kamigaichi, O. (2004). Jma earthquake early warning, *J. Japan Assoc. Earthquake Eng.* **4,**

Lockman, A. and R. M. Allen (2005). Single station earthquake characterization for early warning, *Bull. seism. Soc. Am.* **95,** 2029-2039.

Lockman, A. and R. M. Allen (in review). Magnitude-period scaling relations for japan and the pacific northwest: Implications for earthquake early warning, *Bull. Seismol. Soc. Am.*

Lomax, A. (2005). A reanalysis of the hypocentral location and related observations for the great 1906 california earthquake, *Bull. Seismol. Soc. Am.* **95,** 861-877.

Nakamura, Y. (1984). Development of earthquake early-warning system for the shinkansen, some recent earthquake engineering research and practice in japan, *The Japanese National Committee of the international Association for Earthquake Engineering* **June 1984,** 224-238.

Nakamura, Y. (2004). Uredas, urgent earthquake detection and alarm system, now and future, *Proc. 13th World Conf. Earthquake Eng.* **August 2004,** Paper No. 908.

Odaka, T., K. Ashiya, S. Tsukada, S. Sato, K. Ohtake and D. Nozaka (2003). A new method of quickly estimating epicentral distance and magnitude from a single seismic record, *Bull. Seismol. Soc. Am.* **93,** 526-532.

Olson, E. and R. M. Allen (2005). The deterministic nature of earthquake rupture, *Nature* **438,** 212-215.

Richter, C. F. (1958). Elementary seismology, *Journal* 768.
Sleeman, R. and T. van Eck (1999). Robust automatic p-phase picking: An on-line implementation in the analysis of broadband seismogram recordings, *Bull. seism. Soc. Am.* **113,** 265-275.
Working Group on California Earthquake Probabilities (2003). Earthquake probabilities in the san francisco bay region: 2002 to 2031,
Wu, Y.-M. and T.-l. Teng (2002). A virtual subnetwork approach to earthquake early warning, *Bull. Seismol. Soc. Am.* **92,** 2008-2018.
Wu, Y. M., T. C. Shin and Y. B. Tsai (1998). Quick and reliable determination of magnitude for seismic early warning, *Bull. Seismol. Soc. Am.* **88,** 1254-1259.
Wurman, G. and R. M. Allen (2005). Elarms earthquake alarm system: Application in northern california, *AGU Fall Meeting*, San Francisco, California,
Zoback, M. L., R. C. Jachens and J. A. Olson (1999). Abrupt along-strike change in tectonic style: San andreas fault zone, san francisco peninsula, *J. Geophys. Res.* **104,** 10719-10742.

BIBLOIGRAPHY

Papers published during the study period

Olson, E. and R. M. Allen (2005). The deterministic nature of earthquake rupture, *Nature* **438,** 212-215.

Lockman, A. and R. M. Allen (2005). Single station earthquake characterization for early warning, *Bull. seism. Soc. Am.* **95,** 2029-2039.

Papers in press at the conclusion of the study period

Allen, R. M. Probabilistic warning times for earthquake ground shaking in the San Francisco Bay Area, *Seis. Res. Lett.*

Papers in review at the conclusion of the study period

Allen, R. M. The elarms earthquake warning methodology and application across california, in *Seismic early warning* eds P. Gasparini and J. Zschau, Springer.

Grasso, V. F. and R. M. Allen. Uncertainty in real-time earthquake hazard predictions.

Lockman, A. and R. M. Allen. Magnitude-period scaling relations for Japan and the Pacific Northwest: Implications for earthquake early warning, *Bull. Seismol. Soc. Am.*

Abstracts and presentations during the study period

Allen, R.M. Earthquake early warning in California. USGS Menlo Park Earthquake Hazards Team Seminar, California.

Allen, R.M. ElarmS methodology and application across California. Institute of Earth Sciences, Academia Sinica. Taipei, Taiwan.

Allen, R. M. Earthquake early warning in northern California, *EERI/ISSS First International Conference on Urban Disaster Reduction*, Kobe, Japan.

Allen, R. M. Application of ElarmS across California, *Earthquake early warning workshop*, Caltech, California.

Allen, R.M. Earthquake early warning. ANSS Advisory Committee.

Allen, R. M. The relation between rupture initiation and earthquake magnitude, *AGU Fall Meeting*, San Francisco, California.

Allen, R. M. and E. L. Olson. The deterministic nature of earthquake rupture? *Chapman Conference: Radiated Energy and the Physics of Earthquake*, Portland, Maine.

Allen, R.M. Earthquake warning in northern California. Annual NEHRP meeting for northern California.

Grasso, V. F. and R. M. Allen. Earthquake warning systems: Characterizing prediction uncertainty, *AGU Fall Meeting*, San Francisco, California.

Wurman, G. and R. M. Allen. ElarmS earthquake alarm system: Application in northern California, *AGU Fall Meeting*, San Francisco, California.

APPENDIX A

Probabilistic warning times for earthquake ground shaking in the San Francisco Bay Area

Richard M. Allen

University of California Berkeley, Department of Earth and Planetary Science

Electronic supplement:

http://seismo.berkeley.edu/~rallen/pub/2005wtpdfsf/esup/

Accepted for publication in Seismological Research Letters

Corresponding author: Richard M. Allen, rallen@berkeley.edu, Tel: 510 642 1275, Fax: 510 643 5811. Department of Earth and Planetary Science, University of California Berkeley, 307 McCone Hall, Berkeley, CA 94720-4767, USA.

Introduction

Current earthquake mitigation in the United States focuses on long-term characterization of the likely levels of ground shaking and the frequency of occurrence (Frankel *et al.*, 1996). These estimates are the basis for building codes which aim to prevent collapse during earthquakes. In other countries, including Mexico, Japan, Taiwan and Turkey, earthquake warning systems (EWS) are used in addition to building codes to further reduce the impact of earthquakes (Espinosa Aranda *et al.*, 1995; Wu *et al.*, 1998; Wu and Teng, 2002; Erdik *et al.*, 2003; Odaka *et al.*, 2003; Boese *et al.*, 2004; Kamigaichi, 2004; Nakamura, 2004; Horiuchi *et al.*, 2005; Wu and Kanamori, 2005). Short-term mitigation actions are taken to reduce both financial losses and casualties.

Earthquake warning systems (EWS) rapidly detect the initiation of earthquakes and warn of the forthcoming ground shaking. For a specific city, such as San Francisco, the warning time could be tens of seconds for some earthquakes but essentially zero seconds for others. However, even in situations when San Francisco gets zero seconds warning, neighboring cities such as Oakland would likely get a few seconds and San Jose would get ~15 sec warning. Thus, for any earthquake scenario in a densely populated region, such as the San Francisco Bay Area (SFBA), an EWS could provide warning to at least some of the affected population in a damaging earthquake.

Here I present estimates of the warning times that would be available for locations across the SFBA if an EWS were implemented in northern California. These warning times are calculated for identified likely earthquake scenarios in northern California. For each scenario an estimate of the probability of occurrence has been made (WGCEP, 2003) allowing calculation of probabilistic warning times. The warning times were calculated using the existing seismic network geometry in the region and are based on the ElarmS methodology for earthquake warning (Allen, 2004).

ElarmS

The ElarmS methodology (Allen, 2004) is designed to predict the distribution of peak ground shaking across the region affected by an earthquake before the beginning of significant ground motion (see http://www.ElarmS.org). This is possible using the first energy to arrive at the surface during an earthquake, the P-waves, which are generally low energy and do not cause damage. It is the later S-waves, which travel more slowly, that cause most damage during earthquakes. The P-wave arrival times at several seismic stations close to the epicenter can be used to locate the earthquake. The magnitude of the earthquake can be estimated from the frequency content of the first four seconds using the method first described by Nakamura (1988). The maximum predominant period observed within 4 sec scales with magnitude of the event. This has been observed for earthquakes with magnitude ranging from 3.0 to 8.3 from several regions around the world (Allen and Kanamori, 2003; Olson and Allen, 2005; Lockman and Allen, 2005; in review). These datasets include events that occurred on extensive strike-slip faults like those in northern California, i.e. the Landers (June 28, 1992; M_w 7.3), Hector Mine (October 16, 1999; M_w 7.1) and Denali (November 3, 2002; M_w 7.9) earthquakes. The accuracy of magnitude estimates are a function of the number of stations providing P-wave data. Datasets from both southern California (Allen and Kanamori, 2003) and Japan (Lockman and Allen, in review) show that using just the closest station to the epicenter the average magnitude error is ~0.75 magnitude units. Once data from the closest 2 stations is available the error drops to ~0.6, and to ~0.5 magnitude units once data from 4 stations are available.

Given the location and magnitude of an earthquake, ElarmS estimates the spatial distribution of peak ground shaking using attenuation relations designed for the purpose (Allen, 2004). One second after the first P-wave arrival at the station closest to the epicenter the first estimate of magnitude is available and the attenuation relations provide peak ground acceleration (PGA) as a function of distance from the epicenter. An "AlertMap" showing the distribution of ground shaking hazard can then be generated. As time progresses, more of the P-wave arrival at the closest station, plus P-

waves from other stations, become available and the magnitude estimate is updated along with the AlertMap. The accuracy of the hazard prediction therefore increases with time while the warning time available decreases.

Warning time estimates

Here, I calculate the distribution of warning times for many likely earthquakes in northern California. A threshold at which a warning is issued is chosen based on the accuracy of the warning. I use the point in time when 4 sec of P-wave data are available at four seismic stations. This point in time is defined as the "alert time" and represents the time when the average error in the magnitude estimate will be 0.5 magnitude units. The warning time is then the difference between the alert time and the estimated time of peak ground shaking for a given location. For the arrival-time of peak ground shaking as a function of epicentral distance I use the S-wave arrival-time curve out to a distance of 150 km and then a constant moveout of 3.55 km/s based on the observed moveout of peak ground shaking in California.

Warning times are calculated for a total of 4070 earthquake epicenters. These epicenters were distributed at 1 km intervals along the faults identified as those most likely to cause damaging earthquakes in northern California by the Working Group on California Earthquake Probabilities (WGCEP, 2003). The study identified seven fault systems, each of which has one or more rupture segments, as shown in Figure 1, that can rupture on their own or with adjacent segments. In all, 35 earthquake rupture scenarios were identified and a probability of occurrence within 30 years was estimated for each. The total probability of one or more of these earthquake scenarios (with magnitudes ranging from 5.8 to 7.9) occurring before 2032 was estimated at 84%. Within the SFBA the faults that are most likely to rupture are the San Andreas Fault and the Hayward-Rodgers Creek Fault with probabilities of producing a magnitude 6.7 or greater earthquake of 21% and 27% respectively. The aggregate probability of one or more magnitude 6.7 or

greater earthquakes within the next 30 years (from 2003 to 2032) in the SFBA is estimated to be 62%.

Each of these earthquake scenarios involves rupture across a finite fault plane. The warning time in a given earthquake is dependent on the epicentral location where the rupture initiates. One does not know the likely point of initiation for the 35 scenarios; I therefore accommodate the uncertainty in epicentral location by distributing epicenters at 1 km intervals along each fault. The probability of an earthquake with each epicentral location within one rupture scenario is set equal, and the aggregate probability of all the epicenters is equal to the scenario probability.

Given the epicenter of an earthquake, the alert time is dependent on the relative locations of seismic stations to detect the P-wave arrivals. Several thousand seismic stations are operated in northern California by the California Integrated Seismic Network (CISN) which consists of multiple, complementary seismic networks (see http://www.cisn.org). The ElarmS methodology requires data from continuous broadband seismic instruments. In northern California such instruments are operated by the University of California Berkeley, which contributes a network of 24 stations, each with a broadband velocity seismometer and an accelerometer, and the U.S. Geological Survey, which operates approximately 100 accelerometers, located mostly in the SFBA, and 15 broadband velocity seismometers. In total, there are approximately 140 seismic stations across northern California that could be used in an EWS, Figure 1 and Electronic Supplement.

The alert time for each earthquake epicenter is calculated as the time at which 4 sec of P-wave data are available at the 4 closest continuous broadband stations plus a fixed telemetry and processing delay of 4.5 sec. A 4.5 sec delay accounts for transmission of waveform data from each station to one of the network operation centers, processing time and transmission of the warning to the user community. Given the current seismic infrastructure in northern California the most significant delay is packetization of data before transmission from each station. I introduce a 2.5 sec delay for packetization

which represents the delay at the slowest existing stations. I add 1 sec for transmission to the processing center and 1 sec for transmission of the warning message. The processing time for the data is negligible. The warning time estimates therefore represent what is possible using the existing seismic network hardware. They could be improved through upgrade of telemetry and processing systems as well as the addition of seismic stations.

Warning time probability density function

The warning time probability density function (WTPDF) for the city of San Francisco is shown in Figure 2. This WTPDF is specifically for the Civic Center; however, it does not vary significantly over the rest of the city. For all the likely damaging earthquakes in the region, San Francisco could receive warnings varying from 77 sec down to -8 sec. Negative warning times mean no warning is possible. The most likely warning times are less than 25 sec; however, the WTPDF has a long tail which is due to the San Andreas Fault. In a repeat of the 1906 earthquake, a 450 km long segment of the fault could rupture. If the event nucleates off the Golden Gate, there would be little or no warning for San Francisco. However, assuming that it is equally likely that rupture nucleates anywhere along the fault, it is more likely that the epicenter will be a significant distance from San Francisco. Thus, there could be tens of seconds warning for this most damaging earthquake scenario. It should be noted that the 1906 rupture probably did nucleate off the Golden Gate (Bolt, 1968; Boore, 1977; Zoback *et al.*, 1999; Lomax, 2005). Whether this means that a future rupture would nucleate in the same location is unknown but seems unlikely. An M6 repeating earthquake on the San Andreas fault was identified near Parkfield in the 1980's (Bakun and Lindh, 1985). The previous two events in 1932 and 1966 were remarkably similar with identical epicenters, magnitudes, fault-plane solutions and unilateral southeastward ruptures. The most recent event in the sequence occurred in 2004 and was also M6.0 ruptures the same segment of the fault. However, the epicenter was to the south and unilateral rupture propagated to the northwest (Dreger *et al.*, 2005; Langbein *et al.*, 2005)

In addition to the warning times for each earthquake I also estimate the likely intensity of ground shaking at the warning point, i.e. the Civic Center in the case of Figure 2. These intensities are derived from ShakeMap scenario calculations (WGCEP, 2003). The gray regions in Figure 2 represent earthquakes for which shaking intensity at the Civic Center is less than V on the Modified Mercalli Intensity (MMI) scale (Richter, 1958) and there is unlikely to be damage. Above a MMI V the likely damage increases with the severity of shaking from light (V: unstable objects displaced), to strong (VII: broken furniture and damage to masonry), to violent (IX: masonry seriously damaged or destroyed, frames displaced from foundations).

In the case of the WTPDF for San Francisco, Figure 2, the long tail of large warning times includes a large portion of the earthquake scenarios that will cause violent (MMI > IX) ground shaking. This is because the intensity of ground shaking in a given earthquake depends on the closest distance to the fault rupture while the warning time depends on the distance to the epicenter. Our warning time estimates are conservative in that they represent the traveltime of shear energy directly from the epicenter to the warning point. The true time of peak ground shaking may not occur until the rupture has propagated along the fault to the closest point, which is typically at a velocity less than the shear-wave speed, and radiated energy has traveled from the fault to the warning point at the shear-wave speed.

The probability of one or more earthquakes occurring by 2032 for which more or less than a specific warning time could be available is shown in Figure 3. The full WTPDF for these locations and other cities and sites of engineering interest are included in the Electronic Supplement. Figure 3A shows that there is a 63% probability of one or more earthquakes that will cause some damage (MMI ≥ V) in San Francisco for which a warning would be available, and a 30% chance of a damaging earthquake for which no warning would be available. For the subset of events that cause violent ground shaking (MMI ≥ IX), there is a 3% probability of an earthquake for which > 10 sec of warning could be available, and a 2% chance of < 10 sec warning. It is therefore twice as likely

that warning would be available in a damaging earthquake and more likely than not that more than 10 sec warning would be available before violent ground shaking. The WTPDF for the San Francisco International Airport (Figure 3B) is similar to that for the city, except that the intensity of ground shaking could be greater given the proximity to the San Andreas fault.

The most severe earthquakes for East Bay cities occur on the Hayward-Rodgers Creek fault. Its proximity to cities such as Oakland (Figure 1) make for reduced warning times, but also lower intensities due to the shorter length of the fault. It is still more likely than not that a warning will be available for a damaging earthquake (Figure 3D). Most of the hazard for San Jose comes from the San Andreas fault. As with San Francisco, this means there is a high probability of large warning times for the most damaging earthquakes. There is a 3% probability of an event causing MMI VIII in San Jose for which > 20 sec warning could be available, more than the 2% chance of < 20 sec warning (Figure 3E). In the October 17, 1989, Loma Prieta (M_w 6.9) earthquake Santa Cruz experienced MMI VIII. There is a 7% probability of a similar intensity of ground shaking by 2032 in Santa Cruz, and a 3% chance of similar ground shaking for which > 30 sec warning could be available (Figure 3C). Finally, the rapidly growing urban areas east of the Berkeley Hills, such as Walnut Creek, are as likely to experience damaging ground shaking as San Francisco, although the most severe events have a lower intensity (Figure 3F). As is the case for all locations in the SFBA, Walnut Creek could receive a warning before ground shaking starts for the majority of damaging earthquakes.

Earthquake warnings in California?

An EWS for San Francisco was first suggested by Cooper (1868), who proposed that the telegraph cables radiating from the city could transmit warning ahead of ground shaking. He also noted that this would not work if the center of the "shock" was close to the city, but estimated such a scenario to occur less than 1% of the time. His estimate was not far from our current estimates today. A more recent study by Heaton (1985)

using a theoretical distribution of earthquakes in southern California concluded that there could be more that a minute of warning for the larger, most damaging earthquakes. Here, I come to a similar conclusion using the set of likely earthquakes and existing seismic stations in northern California.

Active early warning systems are now operational in Mexico, Japan, Taiwan and Turkey. Like ElarmS, the systems in Japan use the P-wave arrival to assess hazard. This approach maximizes the warning time, potentially providing warning in the epicentral region (Odaka *et al.*, 2003; Kamigaichi, 2004; Nakamura, 2004; Horiuchi *et al.*, 2005). In Mexico, the earthquakes which threaten Mexico City are ~300 km away in the coastal region. The Seismic Alert System uses the P- and S-wave energy recorded by seismometers in the epicentral region and transmits the warning ahead of ground shaking (Espinosa Aranda *et al.*, 1995). Other systems are hybrids between these two approaches. In Taiwan, 10 sec of data is used at stations closest to the epicenter (Wu *et al.*, 1998; Wu and Teng, 2002) and development is underway to use the P-wave (Wu and Kanamori, 2005). In Turkey, an amplitude threshold must be exceeded at multiple stations close to the fault to trigger an alert (Erdik *et al.*, 2003; Boese *et al.*, 2004).

The warning messages from these active systems are currently used by transportation systems such as rail and metro systems, as well as private industries, including construction, manufacturing and chemical plants. They are also used by utility companies to shut down generation plants and dams, and emergency response personnel to initiate action before ground shaking. In addition, schools receive the warnings allowing children to take cover beneath desks, housing units automatically switch off gas and open doors and windows, and entire complexes evacuate. Many of these applications would also be appropriate in the SFBA. The WTPDF for the specific location of any user can be calculated to plan automated response. This provides the necessary input for cost benefit analysis of implementation versus anticipated preventable losses over the next 30 year period (Grasso and Allen, in review).

EWS are no panacea for the mitigation of seismic hazard. While EWS cannot warn everyone prior to all ground shaking events, they can offer warning to many affected people most of the time. No approach to natural hazard mitigation is perfect. Building codes are intended to prevent collapse of most structures in most earthquakes. If the mitigation of natural hazards is our intent, it is important to ensure that we continually ask what more could be done, what new technologies can be applied? As the December 26, 2004, tsunami disaster demonstrated most clearly, complacency is not an option. The SFBA has flourished over the last 100 years with few damaging earthquakes. This was not the case in the 100 years prior to the 1906 event, when several moderate to large earthquakes shook the region (WGCEP, 2003). If we are emerging from the stress shadow of the 1906 rupture as the Loma Prieta earthquake may suggest (WGCEP, 2003), we must work hard to expand our mitigation strategies.

Electronic supplement

The electronic supplement includes the warning time probability density functions for 26 locations around the San Francisco Bay Area including cities, airports and other sites of interest. It also includes a map showing all seismic stations and faults included in the analysis.

http://seismo.berkeley.edu/~rallen/pub/2005wtpdfsf/esup/

Acknowledgments

This work benefited from discussions with Michael Brudzinski, David Wald, and the seismic network operators of the CISN, in particular David Oppenheimer, Lind Gee, and Douglas Neuhauser. Support for this work was provided by USGS/NEHRP award 05HQGR0074.

References

Allen, R. M. (2004). Rapid magnitude determination for earthquake early warning, in *The many facets of seismic risk* eds M. Pecce, G. Manfredi and A. Zollo, Universita degli Studi di Napoli "Federico II", Napoli, 15-24.

Allen, R. M. and H. Kanamori (2003). The potential for earthquake early warning in southern california, *Science* **300,** 786-789.

Bakun, W.H. and A.G. Lindh (1985). The Parkfield, California, Earthquake Prediction Experiment, *Science* **229**, 619-624.

Boese, M., M. Erdik and F. Wenzel (2004). Real-time prediction of ground motion from P-wave records, *Eos Trans. AGU Fall Meet. Suppl.* **85,** Abstract S21A.0251.

Bolt, B. A. (1968). The focus of the 1906 California earthquake, *Bull. Seismol. Soc. Am.* **50,** 457-471.

Boore, D. M. (1977). Strong-motion recordings of California earthquake of April 18, 1906, *Bull. Seismol. Soc. Am.* **67,** 561-577.

Cooper, J. D. (1868). Earthquake indicator, *Evening Bulletin* **XXVII**, (23).

Dreger, D. S., L. Gee, P. Lombard, M. H. Murray, and B. Romanowicz (2005), Rapid finite-source analysis and near-fault strong ground motions; application to the 2003 Mw 6.5 San Simeon and 2004 Mw 6.0 Parkfield earthquakes, *Seismo. Res. Lett.*, *76*, 40-48.

Erdik, M. O., Y. Fahjan, O. Ozel, H. Alcik, M. Aydin and M. Gul (2003). Istanbul earthquake early warning and rapid response system, *Eos Trans. AGU Fall Meet. Suppl.* **84,** Abstract S42B.0153.

Espinosa Aranda, J. M., A. Jimenez, G. Ibarrola, F. Alcantar, A. Aguilar, M. Inostroza and S. Maldonado (1995). Mexico City seismic alert system, *Seismo. Res. Lett.* **66,** 42-52.

Frankel, A., C. Mueller, T. Barnhard, D. Perkins, E. V. Leyendecker, N. Dickman, S. Hanson and M. Hopper (1996). National seismic hazard maps, U.S. Geological Survey, Open-File Report 96-532.

Grasso, V.F. and R.M. Allen (in review). Uncertainty in real-time earthquake hazard predictions. *Bull. Seismol. Soc. Am.*

Heaton, T. H. (1985). A model for a seismic computerized alert network, *Science* **228,** 987-990.

Horiuchi, S., H. Negishi, K. Abe, A. Kamimura and Y. Fujinawa (2005). An automatic processing system for broadcasting earthquake alarms, *Bull. Seismol. Soc. Am.* **95,** 708-718.

Kamigaichi, O. (2004). JMA earthquake early warning, *J. Japan Assoc. Earthquake Eng.* **4.**

Langbein, J., R. Borcherdt, D. S. Dreger, J. Fletcher, J. L. Hardebeck, J. R. Murray, R. Nadeau, M. J. Rymer, and J. A. Treiman (2005), Preliminary report on the 28 September 2004, M 6.0 Parkfield, California earthquake, *Seismo. Res. Lett.*, *76*, 10-26.

Lockman, A. and R. M. Allen (2005). Single station earthquake characterization for early warning, *Bull. Seismol. Soc. Am.* **95** (6), 2029-2039, doi: 10.1785/0120040241.

Lockman, A. and R. M. Allen (in review). Magnitude-period scaling relations for Japan and the Pacific Northwest: Implications for earthquake early warning, *Bull. Seismol. Soc. Am.*

Lomax, A. (2005). A reanalysis of the hypocentral location and related observations for the great 1906 California earthquake, *Bull. Seismol. Soc. Am.* **95,** 861-877.

Nakamura, Y. (1988). On the urgent earthquake detection and alarm system (UrEDAS), *Proc. 9th World Conf. Earthquake Eng.* **VII,** 673-678.

Nakamura, Y. (2004). UrEDAS, urgent earthquake detection and alarm system, now and future, *Proc. 13th World Conf. Earthquake Eng.* August 2004, Paper No. 908.

Odaka, T., K. Ashiya, S. Tsukada, S. Sato, K. Ohtake and D. Nozaka (2003). A new method of quickly estimating epicentral distance and magnitude from a single seismic record, *Bull. Seismol. Soc. Am.* **93,** 526-532.

Olson, E. and R. M. Allen (2005). The deterministic nature of earthquake rupture, *Nature* **438**, 212-215, doi:10.1038/nature04214.

Richter, C. F. (1958). *Elementary seismology*, 768 pp., W.H. Freeman.

WGCEP - Working Group on California Earthquake Probabilities (2003). Earthquake probabilities in the San Francisco Bay Region: 2003 to 2031, U.S. Geological Survey, Open-File Report 03-214.

Wu, Y.-M. and H. Kanamori (2005). Experiment on an onsite early warning method for the Taiwan early warning system, *Bull. Seismol. Soc. Am.* **95,** 347-353.

Wu, Y.-M. and T.-l. Teng (2002). A virtual sub-network approach to earthquake early warning, *Bull. Seismol. Soc. Am.* **92,** 2008-2018.

Wu, Y. M., T. C. Shin and Y. B. Tsai (1998). Quick and reliable determination of magnitude for seismic early warning, *Bull. Seismol. Soc. Am.* **88,** 1254-1259.

Zoback, M. L., R. C. Jachens and J. A. Olson (1999). Abrupt along-strike change in tectonic style: San Andreas fault zone, San Francisco peninsula, *J. Geophys. Res.* **104,** 10719-10742.

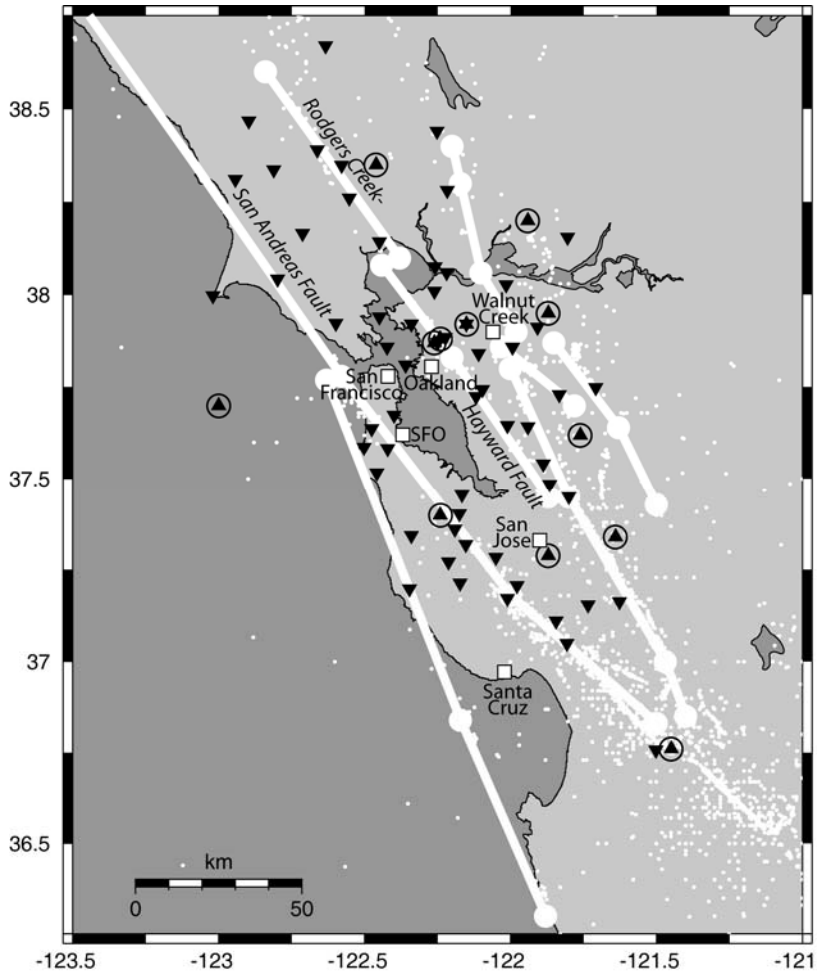

Figure 1. Map of the study region showing existing continuous broadband stations in the Bay Area. Broadband velocity are shown with open circles (operated by UC Berkeley), accelerometers are shown at triangles (UC Berkeley) and inverted triangles (U.S. Geologic Survey). The fault segments identified by the Working Group on California Earthquake Probabilities (WGCEP, 2003) are shown with large white dots at the ends of segments joined by broad white lines. The location of M > 3 earthquakes are shown as small white dots. The six "warning points" included in Figure 2 are shown as white squares.

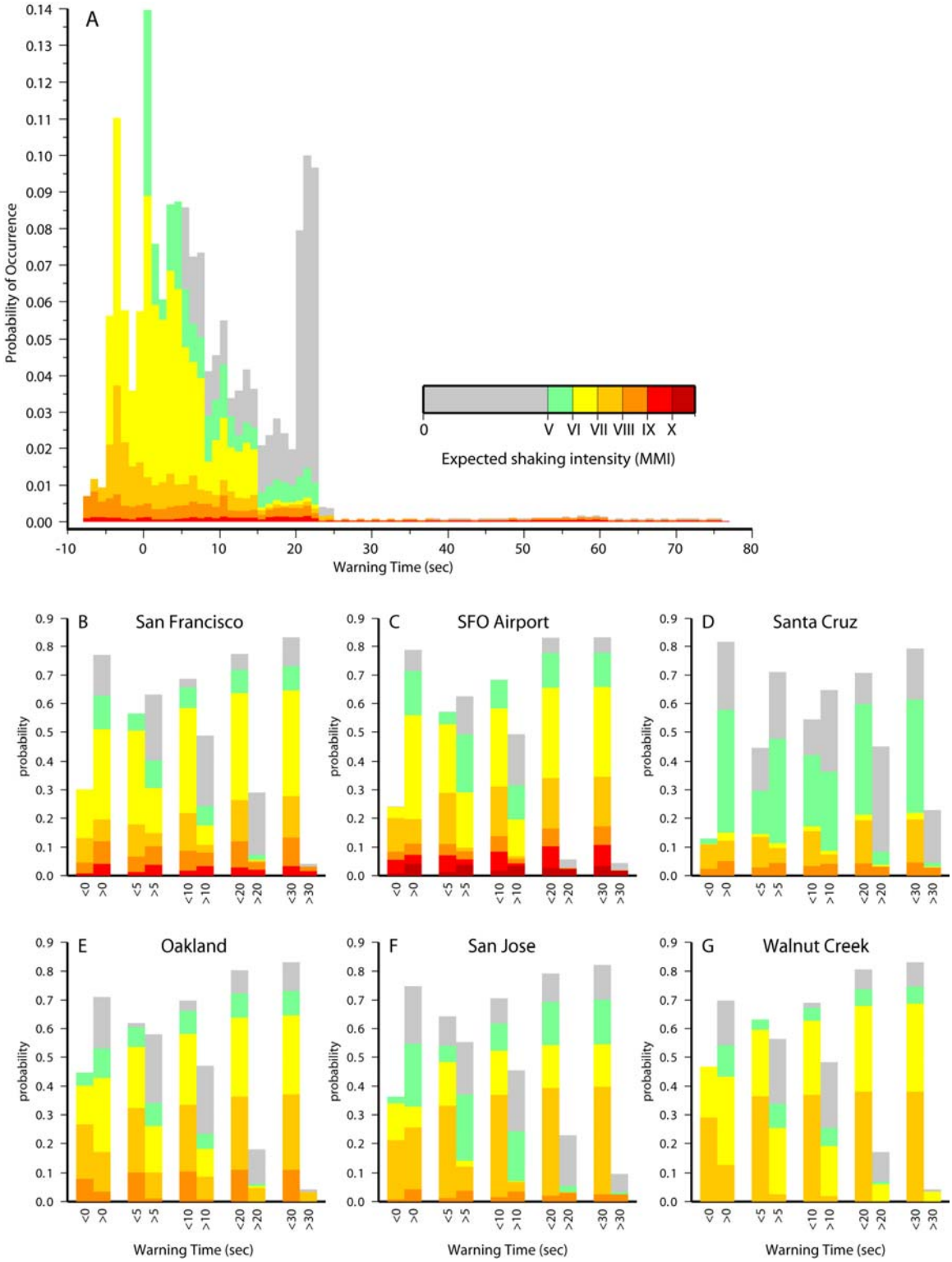
A
Probability of Occurrence
Warning Time (sec)
0
V VI VII VIII IX X
Expected shaking intensity (MMI)
B San Francisco
C SFO Airport
D Santa Cruz
E Oakland
F San Jose
G Walnut Creek
probability
<0 >0
<5 >5
<10 >10
<20 >20
<30 >30
Warning Time (sec)

Figure 2. Warning time distributions. (A) Warning time probability density function (WTPDF) for the Civic Center of San Francisco. The warning times for all likely earthquakes range from -8 sec to 77 sec, where negative warning times mean no warning is possible. Earthquakes are in 1 sec bins and the vertical axis shows the total probability of one or more earthquakes occurring before 2032 with a given warning time. The color represents the estimated intensity of ground shaking for each event. Damage is unlikely for MMI < V (grey); MMI > IX means violent shaking likely to cause serious damage to buildings (red). (B) Probability that one or more earthquakes will occur by 2032 for which more or less than 0, 5, 10, 20 and 30 sec warning time can be available for the city of San Francisco. The color indicates the intensity of ground shaking expected. (C) Probabilistic warning times for San Francisco International Airport, SFO, (D) Santa Cruz, (E) Oakland, (F) San Jose, (G) Walnut Creek. The locations of the five cities and airport are indicated on Figure 1. The full WTPDF are included in the Electronic Supplement along with other locations.

APPENXIX B

Uncertainty in real-time earthquake hazard predictions

Veronica F. Grasso [1,2]
Richard M. Allen [1]

[1]University of California Berkeley, Department of Earth and Planetary Science
[2]University of Naples "Federico II", Department of Structural Analysis and Design

Submitted to BSSA

Corresponding author: Richard M. Allen, rallen@berkeley.edu, Tel: 510 642 1275, Fax: 510 643 5811. Department of Earth and Planetary Science, University of California Berkeley, 307 McCone Hall, Berkeley, CA 94720-4767, USA.

Abstract

Rapid assessment of the hazard posed by an earthquake can be used to provide information on the likely intensity of ground shaking a few seconds to a few tens of seconds before the onset of significant ground shaking. Such earthquake warning systems provide a mechanism for implementing short-term mitigation of the effects of earthquakes. An estimate of the uncertainty in the prediction is equally important to ensure that the cost of taking mitigating action is not greater than the costs associated with the ground shaking. Here we develop a framework for the errors associated with one warning methodology, ElarmS. The errors associated with each system component are assessed using a dataset of earthquakes from southern California. We find that the largest source of error in the predicted peak ground acceleration (PGA) is the attenuation relations which provide PGA given the location and magnitude of an earthquake. The uncertainty in the magnitude estimate derived from the frequency content of P-wave arrivals is less significant, though important in the first 5-10 seconds of an alarm sequence. The location error is insignificant. At a given facility, the threshold at which mitigating actions should be taken can be determined from a cost benefit analysis. First, the costs of taking action should the ground shaking not exceed the predicted level and the cost of not taking action if it does exceed that level must be determined. They can be used to define the threshold, in terms of the probability of a false alarm, at which mitigating action should be taken in order to minimize the costs of earthquakes to the facility. The error model developed here provides the probability of a false alarm.

Introduction

Earthquake warning systems (EWSs) represent a relatively new approach to seismic risk reduction. They provide a rapid estimate of seismic parameters such as magnitude and location associated with an event. This information can then be used to predict ground motion parameters of engineering interest including peak ground acceleration and spectral acceleration. EWS are currently operational in Mexico, Japan, Taiwan and Turkey (Espinosa Aranda *et al.*, 1995; Wu *et al.*, 1998; Wu and Teng, 2002; Erdik *et al.*, 2003; Odaka *et al.*, 2003; Boese *et al.*, 2004; Kamigaichi, 2004; Nakamura, 2004; Horiuchi *et al.*, 2005). They use a variety of techniques to asses the hazard associated with an earthquake and currently forward the warning information to users including transportation systems, private industries, public buildings including schools and government offices, and private residences.

There is an inevitable trade off between the amount of warning time available and the accuracy of the ground shaking prediction. For a given user the point at which mitigating action should be taken has to be determined taking into account the user's requirements. In this paper we focus on estimating the uncertainty in a ground shaking prediction. Good estimates of the uncertainty are important in order to determine the feasibility of any EWS application (Grasso *et al.*, in prep). The decision by an individual user to take action based on a warning message should be based on the expected consequences of the forthcoming ground shaking and the uncertainty in the predicted intensity of the ground shaking. By direct comparison of costs and benefits, expressed in terms of loss of lives, casualties, or economic units, a cogent decision can be made.

The ElarmS methodology (http://www.ElarmS.org) as applied in southern California (Allen and Kanamori, 2003; Allen, 2004) is analyzed as a case study in order to determine the total uncertainty associated with the ground shaking prediction as a time variant parameter. A model of the errors associated with each parameter within the methodology is defined by statistical analysis and a Monte Carlo simulation is used to propagate uncertainties through the system. The analysis allows isolation of component uncertainties

and determination of the main source of uncertainty within ElarmS. This model is then used to define the critical threshold at which a user of the early warning information should initiate mitigating actions based on a cost-benefit analysis. In a real-time application of ElarmS this analysis provides an estimate of the uncertainty in a given prediction at a specific time. In addition, the "future" uncertainty can be estimated to determine if it is likely to reduce significantly within in the next few seconds as more information becomes available. The likely information availability can be estimated from the seismic network configuration and past performance of individual stations.

ElarmS: Real-time ground shaking prediction methodology

The ElarmS methodology is designed to provide the most rapid assessment of the hazard posed by an earthquake as possible. A first hazard estimate is possible one second after the first P-wave trigger. By using the information contained within the P-wave a warning may be issued before significant ground shaking occurs at the surface, i.e. before the S-wave at the epicenter. The methodology is described by Allen and Kanamori (2003) and Allen (2004), here we briefly review the components of the ElarmS methodology that are important in the following error analysis.

Event location is determined from the P-wave arrival times. When the first station is triggered the epicenter is located at that station with a typical depth for the region. When the second station triggers the epicenter is located between the two stations, and then between the first three stations. When four stations have triggered the location is determined by a grid search to minimize residual times using traveltime curves determined from a 1D velocity model for the region (Hauksson, 2000).

Magnitude is estimated using scaling relations between the predominant period of the P-wave within the first 4 seconds and event magnitude (Nakamura, 1988; Allen and Kanamori, 2003; Lockman and Allen, in press; Olson and Allen, in press; Lockman and Allen, in review). For southern California two scaling relations have been defined (Allen

and Kanamori, 2003). Initially, an event is assumed to be "low" magnitude (3.0 < M < 5.0) and the predominant period of the P-wave is determined from the vertical velocity waveform having low-passed the data (using a recursive real-time filter) at 10 Hz. The magnitude is then estimated from the maximum observed predominant period, $T_{\max}^{p}$, using the relation:

$$M = 6.3 \log\left(T_{\max}^{P}\right) + 7.1 \quad (1)$$

If the magnitude estimate for a given event becomes greater than M 4.5, then $T_{\max}^{p}$ is determined from a waveform that has been low-pass filtered at 3 Hz and the magnitude is estimated from the relation:

$$M = 7.0 \log\left(T_{\max}^{P}\right) + 5.9 \quad (2)$$

The first magnitude estimate is available one second after the first station has triggered. As time progresses and more of the P-wave at the first station is available, the magnitude is updated if $T_{\max}^{p}$ increases. As additional stations trigger the event magnitude is defined as the average of individual station estimates.

Given the event location and magnitude, the distribution of ground shaking is estimated using attenuation relations. Most published attenuation relations focus on large magnitude events (e.g. Newmark and Hall, 1982; Abrahamson and Silva, 1997; Boore *et al.*, 1997; Campbell, 1997; Sadigh *et al.*, 1997; Somerville *et al.*, 1997; Field, 2000; Boatwright *et al.*, 2003). ElarmS is intended to be operational for M > 3 earthquakes and therefore uses its own simplified attenuation relations. The attenuation model used for southern California is defined as:

$$\log_{10} PGA = 0.7179M + 2N - N \log_{10}(R) - 3.2373 \quad (3)$$

where *PGA* is the peak ground acceleration, *M* is the magnitude, *R* is the epicentral distance and *N* is a coefficient which is a function of the magnitude (Allen, 2004).

Sources of uncertainty

We use a dataset of 32 earthquakes from southern California to estimate the errors in ground shaking predictions. In order to assess the uncertainty if ElarmS was implemented in southern California, the event dataset consists of earthquakes recorded by the current dense seismic network close to the metropolitan areas, Figure 1. All the events occurred from 2000 to 2003 and have a local magnitude ranging from 3.0 to 5.4 (Table 1). The dataset does not include larger magnitude earthquakes as none have occurred beneath a dense seismic network as exists today. The waveforms were recorded by the California Integrated Seismic Network (http://www.cisn.org) and were obtained from the Southern California Earthquake Data Center (http://www.data.scec.org).

The ElarmS methodology can be represented as a multi-component model consisting of earthquake location, magnitude estimation and ground shaking prediction. The total uncertainty in a ground motion prediction can be derived from the individual errors in location, magnitude estimates using the predominant period, and the attenuation relations.

Magnitude uncertainty

We determine the error in the ElarmS magnitude estimate as a function of time for the 32 events. The error is defined as the difference between the magnitude estimate using equations (1) and (2) and the true magnitude determined by the network. The time of the first trigger for each event is set to the zero time. In making this choice we assume that the amount of information about an earthquake, i.e. the number of stations recording P-wave information, increases in a similar fashion with time for all earthquakes. This assumption is reasonable for events occurring beneath the dense portion of the seismic network where the station spacing is approximately constant.

The magnitude error follows a Gaussian distribution. For each 1 sec increment an error model is determined by fitting a Gaussian distribution to the errors to determine the mean and standard deviation. Figure 2 shows that the error decreases as a function of time. Initially the magnitude estimate is low and the error large with a mean and standard deviation of -0.45 and 0.61 respectively. Hereafter, we refer to mean and standard deviations as -0.45 ± 0.61. The values decrease to -0.25 ± 0.41 after 5 sec, -0.14 ± 0.34 after 10 sec, and stabilize at -0.05 ± 0.26 at 15 sec (Figure 2 and Table 2). Clearly the greatest improvements in the magnitude estimate occur within the first few seconds as the number of triggered stations increases from 1 due to the $N^{-1/2}$ dependence of the errors, where N is the number of stations providing data. The magnitude estimation methodology is also designed to give lower magnitude estimates initially, which may increase as additional data becomes available (Allen and Kanamori, 2003). This is an effort to minimize false alarms due to uncertain magnitude estimates.

Location Uncertainty

The location error is defined as the scalar distance between the estimated epicenter and the true network epicentral location. We calculate the location errors for the 32 earthquakes at 1 second increments and determine the best fit lognormal distributions. These distributions are shown in Figure 3 and their mean and standard deviations are given in Table 3. We find that the location error is reduced to within 1 km within a few seconds. Given 1 trigger an event is located at the station to trigger which would mean that a typical location error would be ~7 km (given the typical station spacing of 20 km). At 1 sec, however, the error is 1.41 ± 1.02 km which is significantly lower (Table 3). This is because information is assimilated in 1 second increments and the station density results in typically two or three triggers to occur within the first second making for accurate location estimates very quickly.

Attenuation model uncertainty

The attenuation model error is the difference between the predicted peak ground acceleration (*PGA*), estimated with equation (3), and the observed *PGA* recorded during the course of the earthquake. The error in the attenuation relationship represents the error

in the *PGA* prediction given the correct magnitude and distance. The attenuation relationship error follows a Gaussian distribution and the best fit Gaussian to the errors for all 32 earthquakes are shown in Figure 4. The error distributions are similar for all the events, with means around zero, except for one which has a mean of 2.0. This is a M 3.1 earthquake that occured 3/11/2000. For this event all stations that recorded detectable ground shaking were within 10 km. The uncertainty in the attenuation relation predictions are greater at small epicentral distances and in this case predict a substantially higher intensity of ground shaking than occured. The errors for all events are combined to determine a single Gaussian error distribution for the attenuation relations. It has a mean of 0.26 and standard deviation equal to 0.9 (Figure 4).

Error analysis

To simulate the errors in ground shaking predictions generated by ElarmS we propagate the errors through the system. The estimated value of peak ground acceleration, $\hat{PGA}$, is a function of the estimated magnitude, $\hat{M}$, and the estimated epicentral distance, $\hat{R}$:

$$\hat{PGA} = f(\hat{M}, \hat{R}) \tag{4}$$

where *f* represents the attenuation relationship in equation (3). $\hat{M}$ and $\hat{R}$ are estimated from the true magnitude *M*, the true epicentral distance *R*, using their time dependent errors ε_M, ε_R (Figures 2 and 3) respectively:

$$\begin{aligned} \hat{M} &= M + \varepsilon_M \\ \hat{R} &= R + \varepsilon_R \end{aligned} \tag{5}$$

thus

$$\hat{PGA} = f(M + \varepsilon_M, R + \varepsilon_R) \tag{6}$$

The error in the *PGA* prediction, ε_{PGA}, is determined by differencing the logarithm of the observed and the predicted *PGA*:

$$\varepsilon_{PGA} = \log\left(\hat{PGA}\right) - \log\left(PGA\right) = \log\left(f(M + \varepsilon_M, R + \varepsilon_R)\right) - \log\left(PGA\right) \tag{7}$$

We use the difference in the logarithm of the *PGA* observation to account for the wide range of *PGA* values given the range of magnitudes for the dataset. This is typical in studies of ground shaking attenuation.

A Monte Carlo simulation is used to estimate the total uncertainty in ε_{PGA}. The 32 earthquake dataset consists of a total of 2961 observations of *PGA* for which *M* and *R* are known. For each of these data we run 1000 simulations from 1 to 25 seconds. For each time increment $\hat{M}$ and $\hat{R}$ are estimated using equation (5) and randomly choosing errors from their time-dependent distributions to generate $\hat{PGA}$. ε_{PGA} is then calculated using the predicted and observed *PGA*.

The uncertainty associated with the ground motion parameter prediction follows a Gaussian distribution with mean and standard deviation that vary with time as shown in Figure 5 and summarized in Table 4. The mean is low initially due to the conservative estimate of magnitude as described above, but rapidly increases from -0.61 at 1 sec to -0.17 at 5 sec. The standard deviation decreases a little with time from 1.33 at 1 sec to 0.95 at 20 sec.

Sensitivity analysis

To determine the largest source of error in the PGA predictions we conduct a simple sensitivity analysis. The total error in the PGA prediction can be espressed as

$$\varepsilon'_{PGA} = \log\left(f(M+\varepsilon_M, R+\varepsilon_R)+\varepsilon_{Att}\right) - \log\left(f(M,R)\right) \qquad (8)$$

where ε'_{PGA} is the error in the PGA estimate calculated using the error models rather than the observed PGA (which was the case in equation 7), and ε_{Att} is the error in the attenuation relations which is Gaussian with mean 0.26 and standard deviation equal to 0.9 as described above.

We consider four cases. In case 1 we include all three sources of error in equation 8. The characteristics of ε'_{PGA} are shown in Figure 6 and Table 5. The errors are of course very similar to those in Table 4 where the total error was determined by differencing the prediction with the observed PGA. In case 2 we set the error in the magnitude estimate,

ε_M, to zero thereby assuming an exact magnitude is available for an event and ε_R and ε_{Att} are the only sources of error in ε'_{PGA}. Figure 6 and Table 5 show ε'_{PGA} as a function of time. Comparing case 2 to case 1 (Figure 6) the most important difference is that the mean in case 2 is no longer initially low. The low initial estimate in ground shaking is a product of the low initial magnitude estimate which is a design element of ElarmS. The standard deviation in case 2 is 0.9 at all times. This is a marginal improvement on the standard deviation for case 1 at ≤ 10 sec and similar at later times. It is also equal to the standard deviation for the attenuation models.

In case 3 the epicentral distance estimate is assumed to be accurate while ε_M and ε_{Att} are sources of error. Figure 6 and Table 5 show that the errors for case 3 are very similar to case 1 indicating that errors in epicentral distance are not a significant contribution to the overall error. Finally, in case 4 ε_{Att} is set to zero and we consider errors in ε_M and ε_R only. In this case (Figure 6 and Table 5) the mean error parallels the error for case 1 but is always lower starting at -0.91 at 1 sec and increasing to -0.14 at 20 sec. The standard deviation is significantly lower than case 1 except for the first few seconds. This shows that ε_{Att} dominates ε'_{PGA} after 5-10 sec. In summary, ε_R has a negligible contribution to uncertainty in PGA predictions, ε_M contributes initially (the first 5-10 sec), and ε_{Att} is the most significant source of error, particularly at later times after several stations have recoded P-wave arrivals and contribute to the magnitude estimate.

Station- and site- specific errors

In the above analysis it has been assumed that the errors in $\hat{M}$ from individual station observations, and in $\hat{PGA}$ at specific sites are the same. Improvements in the uncertainty of $\hat{PGA}$ can be made by taking both the individual stations and site errors into account. This is particularly important during the first few seconds of an earthquake sequence when data for a magnitude estimate is only available from a few stations. A recent study by Lockman and Allen (in press) determined the variability in the uncertainty in magnitude

estimates from 22 stations in southern California. The average absolute magnitude error for the 22 stations varied from 0.13 to 1.02 magnitude units (see Lockman and Allen (in press) Figure 2), the corresponding range in the standard deviation was 0.18 to 1.57 magnitude units. A magnitude estimate based on observations from the best three stations in the Lockman and Allen study would have a standard deviation of 0.15 compared 0.41 when we treat the errors from all stations as being the same. In the case when it is the worst three stations the standard deviation would be 0.83.

The use of station-specific errors is perhaps most important in the real-time decision making process. Consider a scenario in which a specific user of the warning information receives a message predicting ground shaking above the threshold at which they would take action. When they first receive this warning the uncertainty may be large. However, if they know that 2 sec later, additional data is likely to reduce the uncertainty significantly, they may decide to wait for that information before taking action. Alternatively, if the uncertainty is unlikely to change, they will either initiate mitigating action immediately or not at all. If the first two stations to detect P-wave arrivals are those with the largest errors in Lockman and Allen's study, the magnitude uncertainty would be 1.09. Based on the event location, the small subset of stations which will trigger next will be known along with their associated errors. If the third station to trigger is also a poor station the error will reduce to 0.83, but if it is a good station it will be reduced to 0.7.

Application of warning information

Active earthquake warning systems are now operational in Mexico, Japan, Taiwan and Turkey (Espinosa Aranda *et al.*, 1995; Wu *et al.*, 1998; Wu and Teng, 2002; Erdik *et al.*, 2003; Odaka *et al.*, 2003; Boese *et al.*, 2004; Kamigaichi, 2004; Nakamura, 2004; Horiuchi *et al.*, 2005). Their warning messages are currently used by transportation systems such as rail and metro systems, as well as private industries, including construction, manufacturing and chemical plants. They are also used by utility companies to shut down generation plants and dams, and emergency response personnel to initiate action before ground

shaking. In addition, schools receive the warnings allowing children to take cover beneath desks, housing units automatically switch off gas and open doors and windows, and entire complexes evacuate.

An emerging application of EWS is the structural control of buildings during earthquake ground shaking (Kanda *et al.*, 1994; Mei *et al.*, 2000; Occhiuzzi *et al.*, 2004). Such systems would actively vary the mechanical properties of a building during an earthquake to minimize structural damage. Semi-active structural control systems are intended to respond in a passive fashion to ground shaking and could be activated and "tuned" prior to ground shaking resulting in better performance of the system. EWS may be used to activate such systems and the autonomous power supplies required for continuous operation during the seismic event.

Many of these applications can benefit from a real-time cost benefit analysis to determine at what point during an earthquake action should be taken. As a consequence of the uncertainty associated with the prediction, we may commit errors of two kinds: false and missed alarms. A missed alarm occurs if we do not activate the alarm when we should have activated it. A false alarm occurs when we activate the alarm when we should not have. The performance based approach offers a methodology to optimize the activation threshold (Grasso *et al.*, in prep). The critical threshold, *a*, for a facility is the intensity of ground shaking at which unacceptable damage or injury will occur. The warning threshold at which mitigating actions should be taken is defined as *ca,* where *c* is a coefficient. If false alarms are not a serious concern and the consequences of *PGA* exceeding *a* are, then *c* will be a small number less that one. If the reverse is true and false alarms are highly costly, then *c* should be larger than one. Figure 7 schematically shows the inherent trade-off between false and missed alarms. The total uncertainty, ε'_{PGA}, in the prediction is represented by the width of the data points in Figure 7. *a* and *ca* are indicated on the PGA and $P\hat{G}A$ axes respectively. If the value of *c* is increased then the number of false alarms is reduced but at the cost of increased missed alarms.

At any time during an earthquake the probability of a false, P_{fa}, or missed alarm, P_{ma}, can be calculated given the error distribution of $P\hat{G}A$ (Grasso *et al.*, in prep):

$$P_{fa}(t) = P\left[PGA < a \mid P\hat{G}A(t)\right]$$
$$P_{ma}(t) = P\left[PGA \geq a \mid P\hat{G}A(t)\right] \quad (9)$$

where the probability distribution function $P(PGA \mid P\hat{G}A)$ is a Gaussian distribution with mean $P\hat{G}A + \mu_{\varepsilon'_{PGA}}$ and standard deviation $\sigma_{\varepsilon'_{PGA}}$ given by error analysis. The threshold in terms of tolerable probability of false alarm at which action should be taken can be defined in terms of the ratio of costs of false alarm, C_{fa}, to the savings made by activating the alarm when the ground shaking then exceeds the critical threshold, C_s. We define the threshold, β, in terms of this cost ratio:

$$\beta = \frac{C_s}{C_{fa} + C_s} \quad (10)$$

A facility can minimize the costs associated with earthquakes by activating the alarm and mitigation steps when $P_{fa} < \beta$ The same cost-benefit analysis can be used to define *c*, in which case activating the alarm when $P\hat{G}A > ca$ is equivalent to activating it when $P_{fa} < \beta$.

Summary

Earthquake warning information should include three components: a measure of the predicted intensity of ground shaking, the uncertainty in that prediction, and an estimated time until onset of the ground shaking. Here we have developed the necessary framework to model the uncertainty in the predicted peak ground acceleration using the ElarmS methodology (Allen and Kanamori, 2003; Allen, 2004). Using a set of 32 earthquakes from southern California, models of the distribution of errors associated with each of the system components have been derived and propagated through the system to determine the time-dependent error in the final prediction. The magnitude estimate derived from the

predominant period of the P-wave arrival is found to have a Gaussian distribution which is time dependent. The mean and standard deviation vary from -0.5 ± 0.6 magnitude units at 1 sec, to -0.3 ± 0.5 at 2 sec, to -0.2 ± 0.4 at 6 sec to 0.1 ± 0.3 at 11 sec, reaching 0.0 ± 0.3 at 20 sec after the first trigger. The magnitude estimate is designed to be low initially, and be increased as more data becomes available if it suggests a larger magnitude earthquake. The epicentral distance error is modeled as a lognormal distribution. It has a mean and standard deviation of 1.41 ± 1.02 km at 1 sec and rapidly reduces. Finally, the attenuation relations used to predict PGA given the magnitude and location have a Gaussian shaped distribution with mean and standard deviation of 0.26 ± 0.9. This error is time-invariant and measured as $\log(\hat{PGA}) - \log(PGA)$.

Given these error distributions for the ElarmS components, a Monte Carlo simulation has been used to propagate errors through the system. This complete error model results in a time-dependent Gaussian shaped distribution for the error in the PGA prediction which is consistent with the observed errors for the dataset of 32 earthquakes. A sensitivity analysis shows that the largest source of error is currently the attenuation relations. The error in the magnitude estimate represents an important contribution for the first 5-10 seconds, while the location error is insignificant. This error analysis assumes the same error distribution for magnitude estimated from different stations, and PGA estimates at different locations. Lockman and Allen (in press) have shown that magnitude errors do vary between stations. Improvements to both the accuracy of magnitude estimates and the uncertainty estimates could therefore be made when sufficient data is available. The same is likely true for specific sites where ground motion is predicted.

Given both the predicted PGA and its uncertainty, the probability of a false alarm or missed alarm at a specific facility can be calculated given the ElarmS error model. A cost-benefit analysis can be used to determine the optimal point when mitigating actions should be taken. The analysis requires the cost of taking mitigating actions should ground shaking not reach the predicted level, and the cost saved by taking action before ground shaking reaches the predicted level. By taking actions only when the probability of a false alarm

drops below a level defined by the ratio of these costs, the facility can minimize the overall cost of earthquakes.

Acknowledgements

We thank Gaetano Manfredi and James Beck for their support and encouragement, and Mei Xue for assistance in algorithm development. Funding for this study was provided by USGS NEHRP award 05HQGR0074. The figures were generated using GMT (Wessel and Smith, 1995).

References

Abrahamson, N. A. and W. J. Silva (1997). Empirical response spectral attenuation relations for shallow crustal earthquakes, *Seismo. Res. Lett.* **68,** 94-127.

Allen, R. M. (2004). Rapid magnitude determination for earthquake early warning, in *The many facets of seismic risk* eds M. Pecce, G. Manfredi and A. Zollo, Universita degli Studi di Napoli "Federico II", Napoli, 15-24.

Allen, R. M. and H. Kanamori (2003). The potential for earthquake early warning in southern california, *Science* **300,** 786-789.

Boatwright, J., H. Bundock, J. Luetgert, L. Seekins, L. Gee and P. Lombard (2003). The dependence of pga and pgv on distance and magnitude inferred from northern california shakemap data, *Bull. Seismol. Soc. Am.* **93,** 2043-2055.

Boese, M., M. Erdik and F. Wenzel (2004). Real-time prediction of ground motion from p-wave records, *Eos Trans. AGU Fall Meet. Suppl.* **85,** Abstract S21A.0251.

Boore, D. M., W. B. Joyner and T. E. Fumal (1997). Equations for estimating horizontal response spectra and peak acceleration from western north american earthquakes; a summary of recent work, *Seismo. Res. Lett.* **68,** 128-153.

Campbell, K. W. (1997). Empirical near-source attenuation relationships for horizontal and vertical components of peak ground acceleration, peak ground velocity, and pseudo-absolute acceleration response spectra, *Seismo. Res. Lett.* **68,** 154-179.

Erdik, M. O., Y. Fahjan, O. Ozel, H. Alcik, M. Aydin and M. Gul (2003). Istanbul earthquake early warning and rapid response system, *Eos Trans. AGU Fall Meet. Suppl.* **84,** Abstract S42B.0153.

Espinosa Aranda, J. M., A. Jimenez, G. Ibarrola, F. Alcantar, A. Aguilar, M. Inostroza and S. Maldonado (1995). Mexico city seismic alert system, *Seismo. Res. Lett.* **66,** 42-52.

Field, E. H. (2000). A modified ground-motion attenuation relationship for southern california that accounts for detailed site classification and a basin-depth effect, *Bull. Seismol. Soc. Am.* **90,** S209-S221.

Grasso, V. F., J. L. Beck and G. Manfredi (in prep). Seismic early warning systems: Procedure for automated decision making,

Hauksson, E. (2000). Crustal structure and seismicity distribution adjacent to the pacific and north america plate boundary in southern california, *Journal of Geophysical Research-Solid Earth* **105,** 13875-13903.

Horiuchi, S., H. Negishi, K. Abe, A. Kamimura and Y. Fujinawa (2005). An automatic processing system for broadcasting earthquake alarms, *Bull. Seismol. Soc. Am.* **95,** 708-718.

Kamigaichi, O. (2004). Jma earthquake early warning, *J. Japan Assoc. Earthquake Eng.* **4,**

Kanda, K., T. Kobori, Y. Ikeda and H. Koshida (1994). The development of a pre-arrival transmission system for earthquake information: Applied to seismic response controlled structures, *Proceedings 1st World Conference on Structural Control*, California, USA, IASC **2**

Lockman, A. and R. M. Allen (in press). Single station earthquake characterization for early warning, *Bull. seism. Soc. Am.*

Lockman, A. and R. M. Allen (in review). Magnitude-period scaling relations for japan and the pacific northwest: Implications for earthquake early warning, *Bull. Seismol. Soc. Am.*

Mei, G., A. Kareem and J. Kantor (2000). Real-time predictive control of structures under earthquakes, *Earthquake Engineering and Structural Dynamics* **30,** 995-1019.

Nakamura, Y. (1988). On the urgent earthquake detection and alarm system (uredas), *Proc. 9th World Conf. Earthquake Eng.* **VII,** 673-678.

Nakamura, Y. (2004). Uredas, urgent earthquake detection and alarm system, now and future, *Proc. 13th World Conf. Earthquake Eng.* **August 2004,** Paper No. 908.

Newmark, N. M. and W. J. Hall (1982). Earthquake spectra and design, *Geotechnique* **25,** 139-160.

Occhiuzzi, A., V. F. Grasso and G. Manfredi (2004). Early warning systems from a structural control perspective, *Proceedings Third European Conference on Structural Control, 3ECSC*, Vienna University of Technology, Vienna, Austria,

Odaka, T., K. Ashiya, S. Tsukada, S. Sato, K. Ohtake and D. Nozaka (2003). A new method of quickly estimating epicentral distance and magnitude from a single seismic record, *Bull. Seismol. Soc. Am.* **93,** 526-532.

Olson, E. and R. M. Allen (in press). The deterministic nature of earthquake rupture, *Nature*

Sadigh, K., C. Y. Chang, J. A. Egan, F. Makdisi and R. R. Youngs (1997). Attenuation relationships for shallow crustal earthquakes based on california strong motion data, *Seismo. Res. Lett.* **68,** 180-189.

Somerville, P. G., N. S. Smith, R. W. Graves and N. A. Abrahamson (1997). Modification of empirical strong motion attenuation relations to include the amplitude and duration effects of rupture directivity, *Seism. Res. Lett.* **68,** 199-222.

Wessel, P. and W. H. F. Smith (1995). New version of the generic mapping tools released, *Supplement EOS Trans. Amer. Geophy. Union* **76,** 329.

Wu, Y.-M. and T.-l. Teng (2002). A virtual subnetwork approach to earthquake early warning, *Bull. Seismol. Soc. Am.* **92,** 2008-2018.

Wu, Y. M., T. C. Shin and Y. B. Tsai (1998). Quick and reliable determination of magnitude for seismic early warning, *Bull. Seismol. Soc. Am.* **88,** 1254-1259.

Department of Earth and Planetary Science,
University of California Berkeley,
307 McCone Hall,
Berkeley, CA 94720-4767, USA.
(R.A.)

Departimento di Analisi e Progettazione Strutturale
Università degli Studi di Napoli “Federico II”
Napoli, Italia
(V.G.)

Table 1. Earthquakes used in the analysis.

Date	Time	Magnitude	Latitude	Longitude	Depth	Number of stations	SCEDC event ID
02/21/00	13:49:43.10	4.3	34.047	-117.255	15.0	40	9140050
03/11/00	21:46:07.80	3.1	33.839	-117.744	3.5	7	9142593
09/16/00	13:24:41.30	3.2	33.976	-118.424	12.2	29	9163314
01/14/01	02:26:14.00	4.3	34.284	-118.404	8.8	55	9613229
01/14/01	02:50:53.00	4.0	34.289	-118.403	8.4	49	9613261
02/10/01	21:05:05.70	5.1	34.289	-116.946	9.1	58	9627721
02/13/01	03:04:35.60	3.5	34.289	-116.942	6.2	42	9628901
02/18/01	06:09:32.10	3.3	33.675	-116.809	16.7	47	9630113
03/25/01	00:41:25.20	3.4	34.048	-117.570	7.5	54	9639729
04/13/01	11:50:12.40	3.6	33.878	-117.688	3.6	59	9644101
04/20/01	09:52:12.20	3.4	33.705	-116.776	16.9	37	9645945
05/14/01	17:13:30.20	3.8	34.226	-117.440	8.7	63	9652545
07/03/01	11:40:48.10	3.9	34.264	-116.764	3.3	47	9666905
08/20/01	07:34:23.10	3.0	34.044	-117.250	15.7	45	9696461
09/09/01	23:59:18.00	4.2	34.059	-118.388	7.9	58	9703873
09/17/01	01:14:49.00	3.1	33.922	-117.774	11.8	40	9706897
09/23/01	22:44:32.00	3.0	33.509	-116.513	15.1	19	9708393
10/28/01	16:27:45.50	4.0	33.922	-118.270	21.1	60	9716853
10/28/01	16:29:54.60	3.0	33.929	-118.296	23.6	41	9716861
10/31/01	07:56:16.60	5.1	33.508	-116.514	15.2	45	9718013
01/29/02	05:53:28.90	4.2	34.361	-118.657	14.2	52	9753485
01/29/02	06:00:39.80	3.9	34.370	-118.668	14.2	52	9753489
01/29/02	06:08:01.80	3.8	34.365	-118.664	14.4	49	9753497
01/29/02	20:23:07.00	3.6	34.363	-118.667	12.6	45	9753949
01/30/02	18:47:57.30	3.5	34.366	-118.661	12.8	40	9755013
03/17/02	05:50:43.10	3.2	33.873	-117.856	9.5	38	12663484
04/05/02	08:02:56.00	4.4	34.524	-116.295	5.6	31	9775765
07/01/02	22:03:59.60	3.3	34.103	-116.651	10.0	33	9796589
09/03/02	07:08:51	4.8	33.917	-117.776	12.9	68	9818433
12/14/01	12:01:35	4.0	33.955	-117.746	13.8	70	9735129
02/22/03	12:19:10	5.4	34.310	-116.848	1.2	67	13935988
03/15/03	10:01:47	3.6	34.310	-116.843	3.8	41	13947424

Table 2. Distribution of magnitude error as a function of time. The errors have a Gaussian distribution characterized by mean, μ, and standard deviation, σ, for each increment of time. The distributions are shown in Figure 2.

t	μ	σ
1 s	-0.45	0.61
2 s	-0.3	0.47
3 s	-0.28	0.47
4 s	-0.28	0.46
5 s	-0.25	0.41
6 s	-0.2	0.39
7 s	-0.19	0.39
8 s	-0.18	0.37
9 s	-0.16	0.37
10 s	-0.14	0.34
11 s	-0.096	0.3
12 s	-0.08	0.26
13 s	-0.067	0.26
14 s	-0.06	0.26
15 s	-0.05	0.26
20 s	-0.045	0.26
25 s	-0.045	0.26

Table 3. Distribution of epicentral distance error as a function of time. The erros have a lognormal distribution with mean, μ, and standard deviation, σ, for each time increment. The distributions are shown in Figure 3.

t	μ	σ
1 s	1.41	1.02
2 s	0.83	0.88
3 s	0.59	0.66
4 s	0.37	0.75
5 s	0.19	0.83
6 s	0.15	0.82
7 s	0.075	0.76
8 s	0.06	0.76
9 s	0.06	0.76
10 s	0.07	0.76
11 s	0.07	0.76
12 s	0.07	0.76
13 s	0.07	0.76
14 s	0.09	0.79
15 s	0.09	0.79
20 s	0.09	0.79
25 s	0.09	0.79

Table 4. Distribution of the total uncertainty in PGA predictions, ε_{PGA}, as a function of time for the 32 earthquakes in the dataset. The erros are Gaussian in shape and characterized by the mean, μ, the standard deviation, σ. The average absolute deviation, aad, and root mean squared, rms, of the errors are also included.

t	μ	σ	aad	rms
1 s	-0.61	1.33	1.15	1.5
5 s	-0.17	1.1	0.86	1.1
10 s	0.01	1.02	0.78	1.02
15 s	0.16	0.95	0.73	0.95
20 s	0.16	0.95	0.73	0.95
25 s	0.16	0.95	0.73	0.95

Table 5. Distribution of errors in the predicted PGA using the ElarmS error model, ε'_{PGA}. For each case the errors have a Gaussian distribution with mean, μ, the standard deviation, σ. The average absolute deviation, aad, and root mean squared, rms, of the errors are also shown. Case 1 is the total error in PGA which includes errors in the magnitude, ε_M, the epicentral distance, ε_R, and the attenuation relations, ε_{Att}. In Case 2 ε_M is set to zero and errors in ε_R and ε_{Att} only are considered. In Case 3 ε_R is set to zero, ε_M and ε_{Att} only are considered. In Case 4 ε_{Att} is set to zero, ε_M and ε_R only are considered.

	Case 1				***Case 2***				***Case 3***				***Case 4***			
t	μ	σ	aad	rms	μ	σ	aad	rms	μ	σ	aad	rms	μ	σ	aad	rms
1 s	-0.66	1.37	1.2	1.52	0.076	0.93	0.74	0.93	-0.48	1.34	1.14	1.43	-0.91	1.03	1.13	1.38
5 s	-0.22	1.12	0.9	1.15	0.18	0.9	0.73	0.92	-0.15	1.125	0.9	1.13	-0.48	0.68	0.67	0.83
10 s	-0.04	1.06	0.85	1.06	0.19	0.9	0.73	0.92	0.03	1.06	0.8	1.06	-0.3	0.56	0.51	0.64
15 s	0.12	0.99	0.8	1	0.19	0.9	0.73	0.92	0.2	0.99	0.8	1	-0.14	0.43	0.36	0.45
20 s	0.12	0.99	0.8	1	0.19	0.9	0.73	0.92	0.2	0.99	0.8	1	-0.14	0.43	0.36	0.45
25 s	0.12	0.99	0.8	1	0.19	0.9	0.73	0.92	0.2	0.99	0.8	1	-0.14	0.43	0.36	0.45

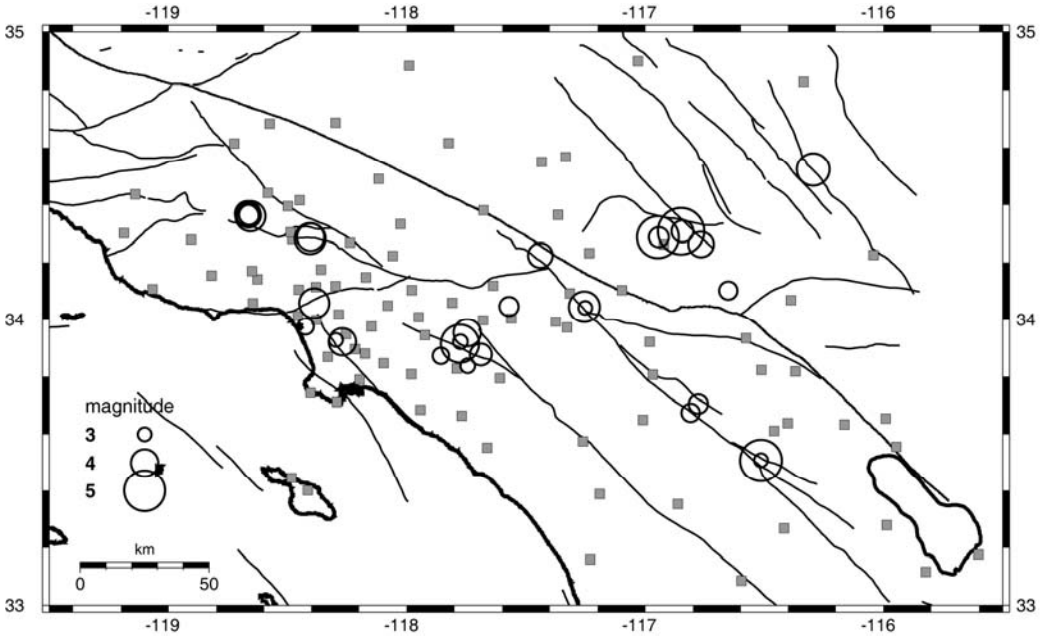

Figure 1. Map of the stations (squares) and earthquakes (circles) used in this study.

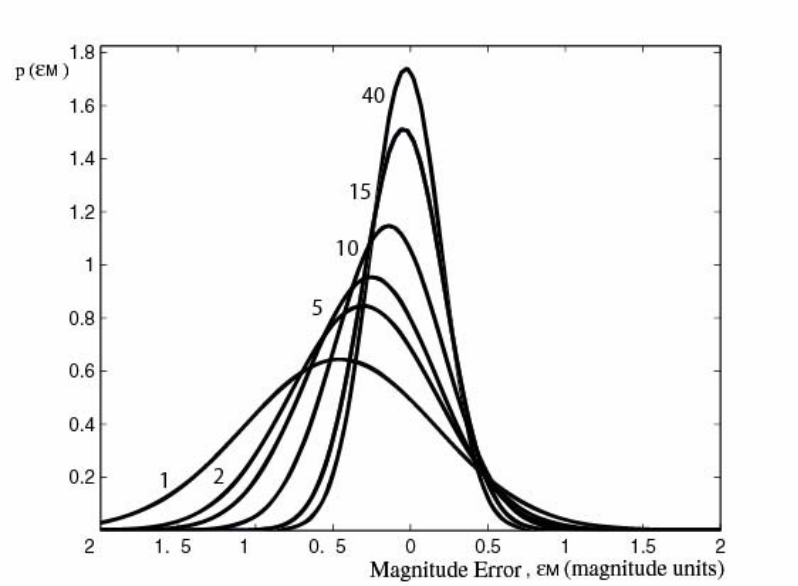

Figure 2. Magnitude error distributions as a function of time. The labels show the time in seconds with respect to the time of the first station to trigger. The mean and standard deviations for each Gaussian distribution are shown in Table 2.

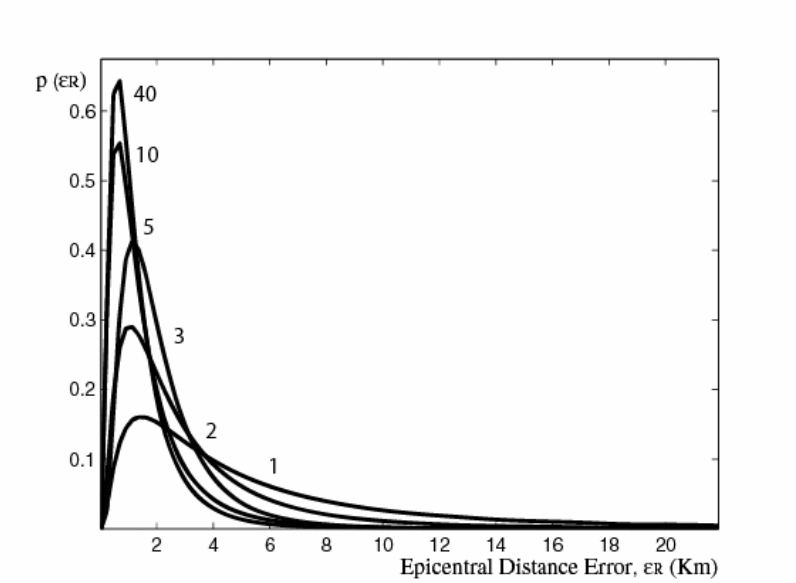

Figure 3. Location error distributions as a function of time. The labels show the time in seconds with respect to the time of the first station to trigger. The mean and standard deviations for each lognormal distribution are shown in Table 3.

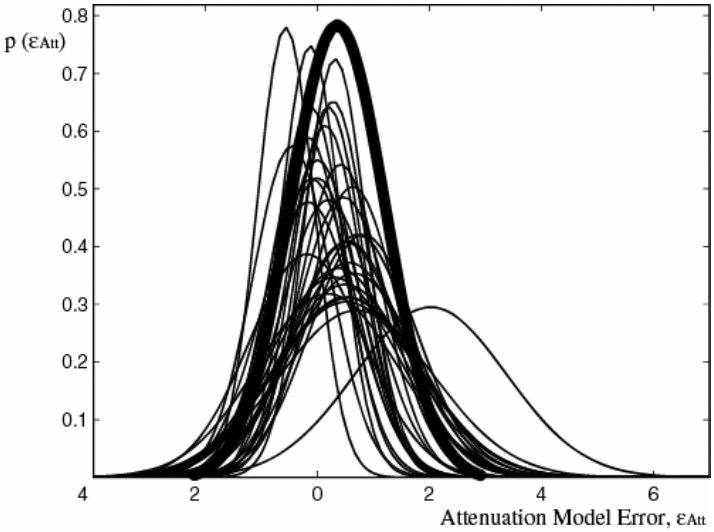

Figure 4. Attenuation model uncertainty. The distributions for each of the 32 earthquakes are shown as thin lines. The distribution for all data is shown as the bold line. See text for definition of attenuation model error.

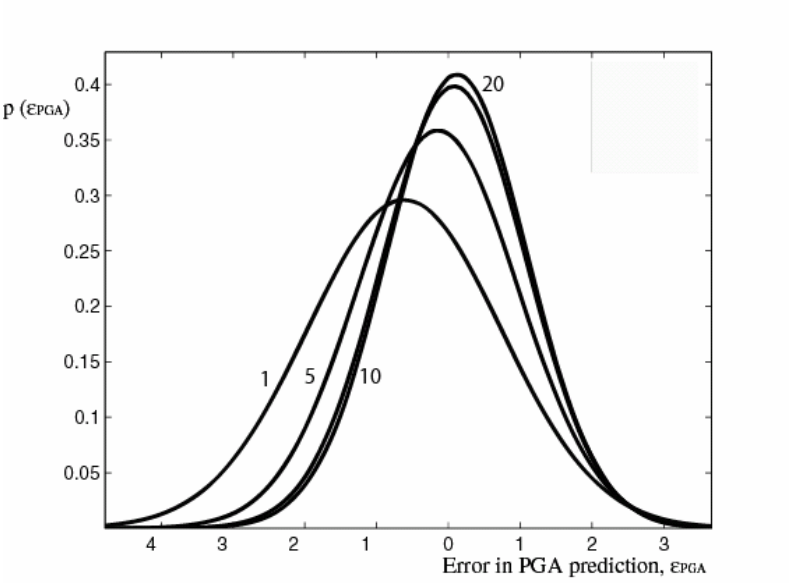

Figure 5. Total error in PGA predictions as a function of time. The labels show the time in seconds with respect to the time of the first station to trigger. The mean and standard deviations for each Gaussian distribution are shown in Table 4.

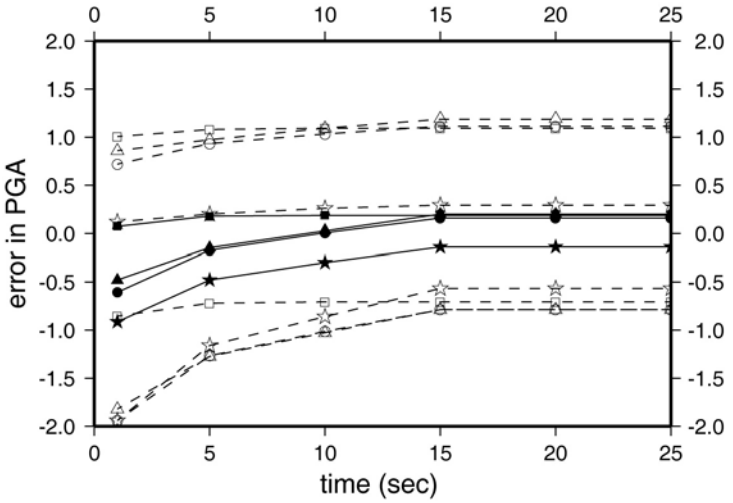

Figure 6. Error in PGA as a function of time for the four cases. The mean is shown as a solid symbol joined by a solid line, plus and minus one standard deviation are shown with open symbols joined by a dashed line. Case 1 (circles) includes all sources of error. Case 2 (squares) neglects error in the magnitude estimate, ε_M, but includes epicentral distance error, ε_R, and the attenuation relation error, ε_{Att}. Case 3 (triangles) neglects ε_R but includes ε_M and ε_{Att}. Case 4 (stars) neglects ε_{Att} but includes ε_M and ε_R.

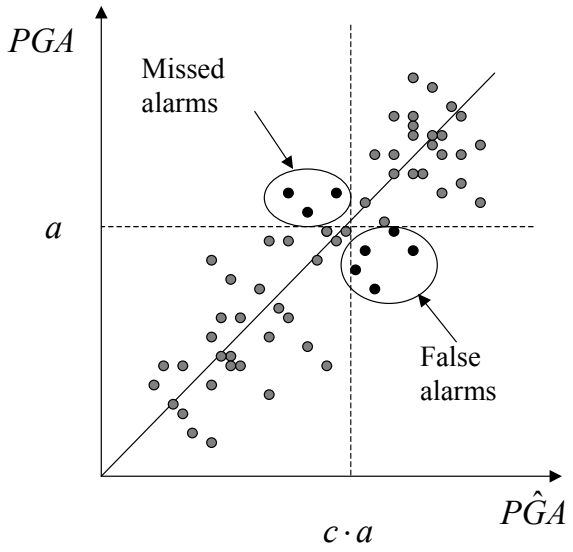

Figure 7. Schematic showing the distribution of errors in *PGA* predictions with respect to the observed *PGA*. The critical threshold, *a*, is shown along with a warning threshold, *ca*. The false and missed alarms are indicated. The number of false alarms can be reduced by increasing the value of *c*. However, the number of missed alarms will also increase.